[redacted]

Coordinated Science Laboratory

UNIVERSITY OF ILLINOIS - URBANA, ILLINOIS

INVESTIGATION OF DENSE PLASMA UNDER A STRONG ELECTRIC FIELD

Clifford W. Mendel, Jr.

REPORT R-289

MAY, 1966

This work was supported wholly by the Joint Services Electronics Program (U. S. Army, U. S. Navy, and U. S. Air Force) under Contract DA 28 043 AMC 00073(E).

INVESTIGATION OF DENSE PLASMA UNDER A STRONG ELECTRIC FIELD

Clifford William Mendel, Jr., Ph.D.
Department of Physics and Coordinated Science Laboratory
University of Illinois, 1966

Abstract

A hydrogen plasma of density $\sim 10^{16}$ cm^{-3} and electron temperature $\sim$ 200 eV has been investigated under electric fields of 100 to 500 V/cm. A pinch of pinch ratio $\sim$ 3 was found to be hydrodynamically stable for $\sim$ 2 μs during which the experiment was performed. A sharp burst of runaway electrons of total current of the order of amperes occured and disappeared shortly after conduction began. Large low frequency oscillations believed to be ion-acoustic oscillations appear and give rise to very high resistivities in qualitative agreement with recent theories on plasma conductivity.

Acknowledgments

The author would like to express his gratitude to Professor Manfred Raether for help and guidance in this work. He would also like to thank machinists Garrie Burr, George Bouck, and Bob Bales, the glass blower Bill Lawrence, and the metallurgist Nick Vassos for their help in constructing the experiment, and to Rose Lane for typing the manuscript.

Table of Contents

1. Introduction

This experiment was performed to investigate the possibility of obtaining strong electron runaway in a dense plasma. Runaway electrons are simply electrons moving so fast that the external electric field imposed on the plasma is the dominant force in determining their motion.

The idea of using a plasma for obtaining high current, space charge neutralized particle beams was first suggested by Budker.[1] He pointed out that not only can the plasma prevent a large space charge from building up, but the current of the plasma will tend to constrict itself.

Several experiments along this line have been performed. Most of these have been toroidal discharges.[2,3,4,5] Axial magnetic fields are used to suppress hydrodynamic instability and aid preionization. The toroidal machines operating at low pressure also have betatron fields. The main disadvantage of these toroidal machines is the necessity of confining the runaway electrons to orbits. This limits the energy spread of electrons that are accelerated without leaving the beam.

Typically about 1 ampere of runaway electrons with energies of a few hundred keV are found. These figures are obtained by observing X-rays from the walls of the discharge tubes. The runaway current is always small compared to the conduction current. The X-rays appear as a burst about a microsecond after conduction begins. There is no runaway after this burst.

Measured electron densities varied from 10^{11} to 10^{16} cm^{-3}. Electron temperatures between 10 and 40 eV were measured. Electric fields were about 10 V/cm.

Reasons for the cessation of runaway were either failure to confine the electrons to legitimate orbits, or two stream instabilities.

By using a linear geometry the difficulty of confining particles to orbits can be eliminated. Suprunenko et al [6] conducted an experiment in which electron runaway from a linear discharge was investigated. The impedance of the discharging circuit was rather high so the electric field varied rapidly in time. Hydrogen gas in the pressure range of 0.5 to 300 μ-Hg was used. The discharge constricted to a diameter of about 5 cm. Peak currents were 100 kiloamperes. The electron density was $5 \cdot 10^{14}$ to 10^{16} cm^{-3}. Electron temperatures found from the intensity ratio of a He I and He II line ($\sim$ 10% He was added to the H_2 for this measurement) were about 30 eV. Runaway currents of 250 amperes were mentioned. The paper is not clear on this, but we believe this is for the whole discharge, and not just the detected runaway. Electric fields measured were about 150 to 600 V/cm. This is at the surface of the tube, however, and not along the axis.

2. Theories of Plasma Conduction

The theory of fully ionized plasma under the influence of an electric field has received considerable attention. All of the theories are based upon a number of assumptions and it is usually difficult to design an experiment consistent with them. In our experiments we are interested in the dc conductivity, where we mean by dc, that times are long compared to the reciprocal of natural frequencies of the plasma, the electron and ion plasma frequencies and gyration frequencies.

These theories may be put into two categories conveniently, those theories that assume spatial homogeneity and consider the effect of collisions and those that do not assume spatial homogeneity and neglect collisions.

All of these theories are approximations to Boltzmann's equations plus Maxwell's equations

$$\left.\begin{aligned} \frac{\partial f}{\partial t} + \underline{v} \cdot \frac{\partial f}{\partial \underline{x}} - \frac{e\underline{E}}{m} \cdot \frac{\partial f}{\partial \underline{v}} &= \left(\frac{\partial f}{\partial t}\right)_c \\ \frac{\partial F}{\partial t} + \underline{v} \cdot \frac{\partial F}{\partial \underline{x}} + \frac{e\underline{E}}{M} \cdot \frac{\partial F}{\partial \underline{v}} &= \left(\frac{\partial F}{\partial t}\right)_c \end{aligned}\right\} \tag{2.1}$$

$$\left.\begin{aligned} \nabla \cdot \underline{E} &= 4\pi e \int d^3v \ (F-f) \\ \nabla \times \underline{E} &= 0 \end{aligned}\right\} \tag{2.2}$$

where f is the electron distribution as a function of time t, position $\underline{x}$, and velocity $\underline{v}$, m is the electron mass and F and M the equivalent matters for the ions. $\underline{E}$ is the electric field, e the magnitude of an

electron charge and the subscript c on the derivatives means they represent changes due to collisions.

2.1 Spatially Homogeneous Theories

The simplest theory, and one that has been found valid experimentally for small electric fields, yields the well-known $T_e^{3/2}$ conductivity law. It is easily derived by assuming infinitely massive ions. The first equation can then be replaced by the equation for a Lorentz gas. Then by assuming spatial homogeneity, time independence and a slowly drifting Maxwelliam of electrons, one obtains a resistivity

$$\eta \simeq \frac{4\pi}{3} \frac{m^{\frac{1}{2}} e^2}{(kT_e)^{3/2}} \ell n\, N_D \text{ (esu)} \qquad (2.3)$$

$$\simeq \frac{0.06}{T_e^{3/2}} \text{ } (\Omega \text{ cm})$$

where T_e is expressed in electron volts, as it shall be throughout this paper. This expression has also been derived by using an expansion of the electron distribution in Legendre Polynomials of the cosine of the angle between the velocity $\underline{v}$ and the electric field $\underline{E}_o$. All theories for small fields and computer calculations yield a similar expression to (2.3), differing at most by factors of the order of 2.

The expression (2.3) has been found to be correct for small electric fields in ohmic heating and theta pinch experiments.

The expression (2.3) may be written instead in terms of the drift velocity of the electrons

$$v_d = \frac{E}{E_c} v_e \tag{2.4}$$

where $v_e = \left(\frac{kT_e}{m}\right)^{\frac{1}{2}}$ and $E_c = \frac{e}{\lambda_D^2} \ell n\ N_D$. $\lambda_D = \left(\frac{kT_e}{4\pi\ ne^2}\right)^{\frac{1}{2}}$ is the electron Debye length and N_D is the number of electrons in the Debye sphere. E_c is the critical electric field first used by Dreicer I.[7] Physically, E_c is the electric field which increases the energy of an electron by kT_e in one mean ion-electron collision length. It is seen from this that as the electric field becomes of the same order as E_c the drift is on the order of v_e and the velocities involved in the collisions are appreciably higher than v_e. Since the collision cross section drops rapidly with increasing velocity, the dynamical friction must be appreciably lower. In Paper I Dreicer assumed a drifting Maxwellian of electrons of arbitrary drift velocity and found that the frictional force dropped off very rapidly as the drift velocity approached v_e. From this it appeared for fields larger than E_c, the electrons would all accelerate rapidly along the electric field.

The critical electric field

$$\begin{aligned} E_c &= \frac{e}{\lambda_D^2} \ell n\ N_D \\ &\doteq 1.2 \cdot 10^{-12}\ \frac{n_e}{T_e}\ \text{V/cm} \end{aligned} \tag{2.5}$$

for n_e in cm^{-3} and T_e in eV is seen to be a reasonably small field for most plasmas.

The obvious defect to applying these results to real plasmas was the assumption of a Maxwellian distribution. This was corrected in a subsequent paper by Dreicer II [8] where he assumed a distribution that was only approximately Maxwellian and obtained rates of runaway for $E \ll E_c$. To do this he looked at particle orbits in velocity space under the influence of the electric field and dynamical friction due to ions. From this he found a surface in velocity space outside of which all particles were dominated by the field, and ran away. He then assumed that all particles at this surface (actually at an approximation to this surface) ran away immediately. He then computed the rate that electrons diffuse out to this surface.

This theory gave rates of runaway which were reasonable, but also predicted complete runaway which was not found experimentally.

Electron runaway was investigated by Kruskal and Bernstein [9] in a more rigorous manner, but still assuming a spatially homogeneous Lorentz gas. They divided velocity space into three regions, a region where the electrons are moving slowly so electron-ion collisions dominate the electric field, a fast region where the field dominates the collisions, and a middle connection region where the collisions and the field are both important. They then solved the problem by expansions and matching solutions at the boundaries of the regions.

This theory yields a runaway current as a function of time, but again predicts complete runaway.

2.2 Spatially Inhomogeneous Theories

It appears that for electric fields appreciably larger than E_c, collisions are no longer important. In this case there will be fast drift velocities which will lead to growing plasma waves. If we think of the plasma in the rest frame of the electrons with the ions drifting through them with velocity u, we can find the drag due to plasma oscillations as follows.

It is well known that the drag force on a charged particle passing through a plasma gives an energy loss of

$$\frac{dw}{dt} = 4\pi e^2 \int \frac{d^2\underline{k}}{(2\pi)^3} \frac{\underline{k}\cdot\underline{u}}{k^2} \operatorname{Im} \epsilon^{-1} (\underline{k}, \underline{k}\cdot\underline{u}) \qquad (2.6)$$

where e is the charge and u is the velocity of the particle. ϵ is the dielectric constant. For a particle of charge e and a velocity somewhat bigger than the electron thermal velocity, this equation gives a drag force due to electron plasma oscillations of

$$F \sim e\, E_c \left(\frac{v_e}{u}\right)^2$$

where E_c is again Dreicer's critical electric field. For particles moving more slowly than v_e, electron oscillations do not cause a drag, but if they are moving faster than the ion-acoustic velocity $V_c = \left(\frac{eT_e}{M}\right)^{\frac{1}{2}}$

$$F \sim e\, E_c \frac{\ell n\, T_e/T_i}{\ell n\, N_D} \left(\frac{V_c}{u}\right)^2 .$$

Since $T_e \gg T_i$ this is of the same order as $e E_c \left(\frac{V_c}{u}\right)^2$. It is seen from this that plasma oscillations can cause a drag that also requires the electric field to be much greater than E_c for complete runaway.

A more rigourous method of looking at the effect of plasma oscillations is to use the quasi-linear theory (cf. Drummond and Pines [10]). Field and Fried [11] investigated a plasma using this theory and found that ion acoustic oscillations vastly effected the electron distribution.

They made two different sets of calculations. Collisions were neglected in both. In one they assumed Maxwellian distributions of both ions and electrons with separate temperatures parallel and perpendicular to the electric field and a drift velocity relative to each other. They then averaged the drag force over all particles due to oscillations and used the difference between this and the electric field force to determine the rate of change of drift velocity. The results were a fast rising current for about 10^3 electron plasma oscillation periods and then a sudden drop to a current such that the drift velocity equalled the ion-acoustic velocity.

Their second calculation was less restrictive. The essential difference between it and the first calculation was that the electron distribution was not Maxwellian parallel to the electric field. The mean velocity again rose linearly for a short time and began suddenly to drop. It did not fall to some constant value, however.

2.3 The Present Experiment

The present experiment was designed to match the conditions of these theories as closely as possible. A linear geometry and constant electric field was used. There are, however, still major differences from the assumptions of the theories of plasma in an electric field. The differences are the presence of a magnetic field and the rapid variation of the electron density with time. There is also a spatial variation of the density of course. The effect of either a superimposed magnetic field or the unavoidable self magnetic field may be quite large as the theory of Field and Fried indicates that plasma oscillations with k vectors at angles to the electric field and therefore the magnetic field may be very important. However, other factors prohibit an accurate quantitative comparison to their theory so this additional difference between their theory and our experiment is not important. Qualitative comparisons will, however, be made.

The rapidly varying density is difficult to avoid due to pinching and ionization. After ionization is near 100% the density does not vary much and the critical electric field is still above E_c. Since there are neutrals in the discharge tube the critical electric field should take this into account. Since the total electron mean free path is

$$\frac{1}{\lambda_e} = \frac{1}{\lambda_{ei}} + \frac{1}{\lambda_{eo}}$$

where λ_{ei} is the electron-ion mean free path and λ_{eo} is the electron neutral mean free path, then the critical electric field is

$$E_c = E_{ci} + E_{co}$$

where

$$E_{ci} = \frac{T_e}{\lambda_{ei}} \ , \ \lambda_{ei} = \frac{4\pi}{\ell n \ N_D} N_D \lambda_D$$

$$\doteq 1.2 \cdot 10^{-12} \frac{n_e}{T_e} \qquad (2.7)$$

$$E_{co} = \frac{T_e}{\lambda_{co}} = n_o \sigma_e(T_e) T_e ,$$

where n_o is the H-atom density, $\sigma_e(T_e)$ is the H-electron collision cross section for electrons of energy T_e. $T_e\sigma_e(T_e)$ has a maximum value of about $1 \cdot 10^{-4}$ eV cm around $T_e \sim 100$ eV. Since $n_o \doteq 6.6 \cdot 10^{13} \ p(1-\alpha)$ for p in μ - Hg and α the fraction of ionization

$$E_{co} = \frac{2}{3} (1-\alpha) \ p \ .$$

If we assume $T_e \sim 200$ eV as it is later seen to be

$$E_{ci} = \frac{1}{3} \alpha p$$

$$E_c = \frac{1}{3} \alpha p + \frac{2}{3} (1-\alpha) \ p$$

$$= \frac{2}{3} \ p + \frac{1}{3} \alpha p \sim \frac{2}{3} \ p \ . \qquad (2.8)$$

Thus for $\alpha \sim 1$ the ions dominate and for $\alpha \ll 1$ the neutrals dominate, but the critical electric field is always roughly $\frac{2}{3}$ p V/cm for p in microns if $T_e \sim 200$ eV. Actually at low pressure pinching raises the electron density to such a degree that E_{ci} is greater than that shown. However, it is found later that the electric field is still above E_c.

3. Induction Machine Design

The design of the machine stems from considerations of strong electric field, large total voltage, and fast diffusion of the field into the plasma.

To maintain large total voltage while keeping condensor bank voltage down to a reasonable value dictated a transformer type of arrangement. We designed the machine following the suggestion of Kerst [12] as a coaxial transformer with the discharge down the axis so that inductance could be held down. The radius of the discharge tube was kept small so that the secondary current and thus back emf's would be small, and electric fields large.

3.1 Transformer Design

While the machine is, in fact, one secondary enclosing four primaries, it has an equivalent circuit of one secondary and one primary as shown in Fig. 3.1.

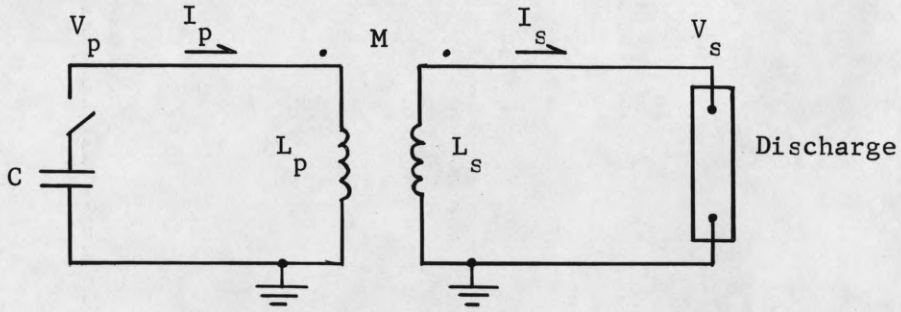

Figure 3.1. Machine Equivalent Circuit.

This circuit obeys the equations:

$$V_p + L_p C \frac{d^2V_p}{dt^2} = - M \frac{dI_s}{dt} \tag{3.1}$$

$$V_s = - MC \frac{d^2V_p}{dt^2} - L_s \frac{dI_s}{dt} = \alpha V_p - L_E \frac{dI_s}{dt} \tag{3.2}$$

where $\alpha = \frac{M}{L_p}$, $L_E = \left(1 - \frac{M^2}{L_s L_p}\right) L_s$. V_p may be written:

$$V_p = V_o \cos \Omega t - \Omega^2 M \int_o^t I(t') \cos \Omega(t-t') \, dt' \tag{3.3}$$

where $\Omega^2 = \frac{1}{L_p C}$ and V_o is voltage on the condensor when the switch is closed at t = o. Therefore:

$$V_s = \alpha V_o \cos \Omega t - L_E \frac{dI_s}{dt} - \frac{M^2}{L_p{}^2 C} \int_o^t I(t') \cos \Omega(t-t') \, dt' . \tag{3.4}$$

The third term will usually be small in our case, as will be seen later. The resistance of the actual machine is neglected since we are only interested in the first quarter cycle.

Consideration of equation (3.2) points to the fact that strong electric field and high voltage tend to contradict each other. This can be seen as follows: the inductance of a coaxial transformer is

$$L = 2\ell \, \ell n \, b/a \quad (m\mu h)$$

where ℓ is the length in cm and b/a is the ratio of inner to outer conductor radii. ℓn b/a varies slowly for $\frac{b}{a} \gg 1$ so that L = const. ℓ for all practical purposes. Therefore let us assume $M = M'\ell$ where M' is a constant. Then, since $L_p - M$ is more or less determined by the condensor bank, ignitrons and coaxial cable

$$\alpha = \frac{V_s}{V_p} = \frac{M}{L_p} = \frac{M'\ell}{(L_p - M) + M'\ell} = \frac{1}{1 + \frac{\ell_o}{\ell}}$$

where $\ell_o = \frac{L_p - M}{M'}$, and

$$E = \frac{V_s}{\ell} = \frac{V_p}{\ell + \ell_o} = \frac{V_p}{\ell_o} \quad \frac{1}{1 + \frac{\ell}{\ell_o}}$$

for $I_s = 0$. Therefore, V_s is greatest for ℓ large compared to ℓ_o and E is large for ℓ small compared to ℓ_o. Before deciding upon a value of ℓ, the variation of L_E with ℓ should be checked.

$$L_E = L_s \left(1 - \frac{M^2}{L_p L_s}\right) = L_s - \frac{M^2}{L_p} = (L_s - M) + M'\ell_o \quad \frac{1}{1 + \frac{\ell_o}{\ell}}$$

$L_s - M$ also has a component proportional to ℓ, as the discharge tube is down the axis of the machine, but this is small compared to $M'\ell_o$ and need not be considered. L_E also increases with ℓ. A value of $\ell \simeq \ell_o$ is a reasonable compromise for all of these parameters. Since $L_p - M \simeq 300$ mμh for the components we used, and 2 ℓn b/a is about 8 mμh/cm for a reasonable sized machine, ℓ = 16 inches $\simeq$ 40 cm was used. Ceramic tubes were easily available in this length.

In the design actually used for the transformers there were four primaries. Each of these consisted of a toroidal section four inches long with a 30-inch outside and 1½-inch inside diameter (Fig. 3.2). The current (actually a negative current) flowed from the condensor, through an ignitron switch mounted in a case on top of the condensor, through low inductance coaxial cable (0.006 mμh/ft) to the primary of the transformer. Here it flowed down a braided copper strap (A in Fig. 3.2) to the center of the transformer, axially along the center (B), out along the primary end place (C), along the 5/8-inch steel supporting rods (D), and back to the coaxial cable outer conductor.

The mutual inductance for these dimensions for the one primary model (that is four times that of one of the actual primaries) can be calculated to be about 300 mμh, including a contribution from the 5/8-inch support rods. This is close to the measured value as will be seen later.

3.2 Discharge Tube Design

The discharge tube must be small enough that back emf's do not lower the voltage too much. Assuming cylindrical symmetry, we have

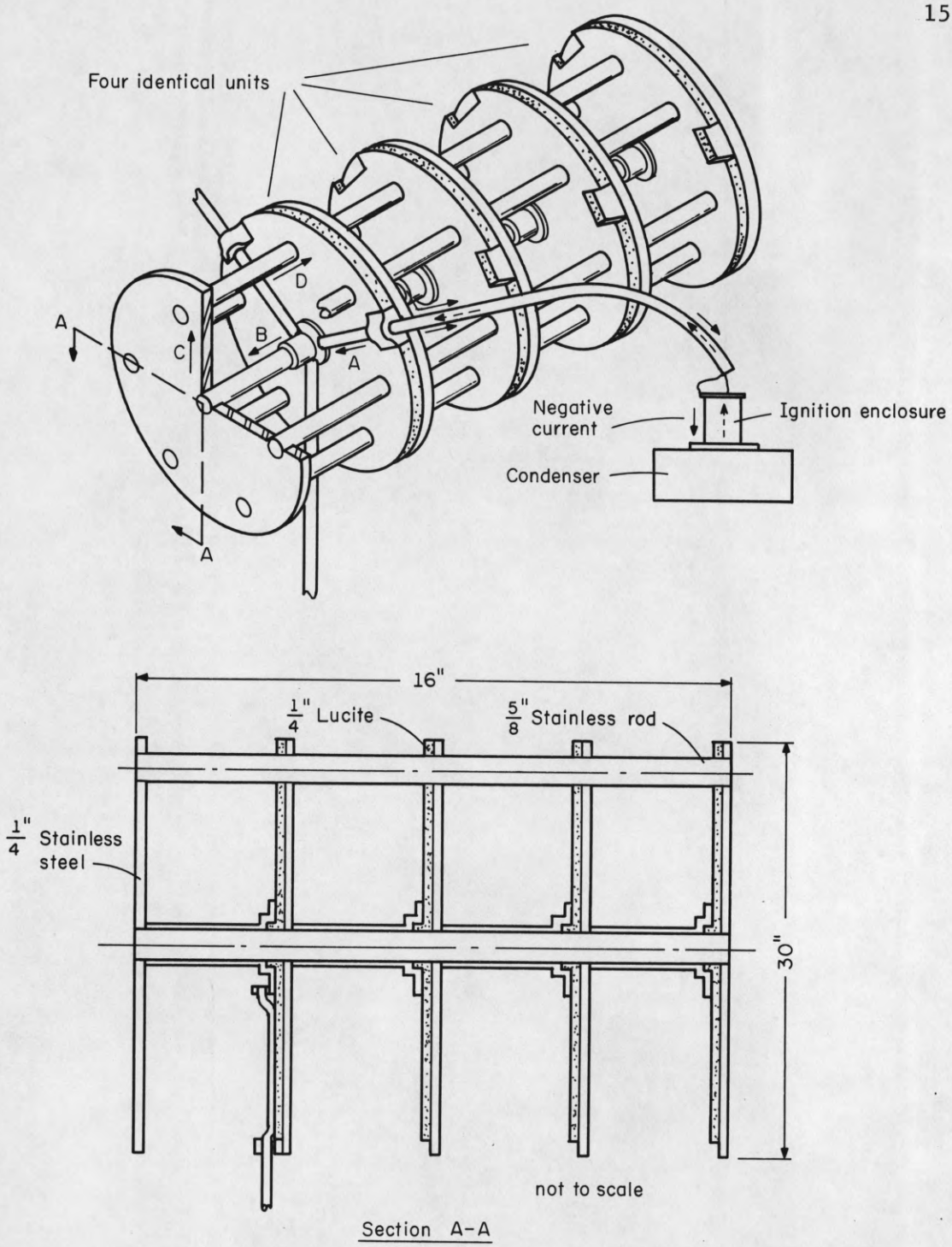

Figure 3.2. Transformer Configuration.

$$\frac{\partial E_z}{\partial r} = \frac{\partial B_\phi}{\partial t}$$

$$V(r_o) - V(o) = \ell \frac{d}{dt} \int_o^{r_o} B_o dr$$

$$= \frac{\mu_o \ell}{2\pi} \frac{d}{dt} \int_o^{r_o} \frac{I(r)}{r} dr \qquad (3.5)$$

where $\hat{z}$, $\hat{r}$, and $\hat{\phi}$ directions are as shown in Fig. 3.3, I(r) is the total current through a disc of radius r centered on and normal to the axis and V(r) is the integral of the electric field down a line parallel to and a distance r from the axis. Assuming the discharge is pinched so that the current density is large inside some radius r_o/K and small outside r_o/K, then

$$\int_o^{r_o} \frac{I(r)}{r} dr \sim I_o \ell n\, K$$

where $I_o = I(r_o)$. K is the pinch ratio and is greater than 1. Then

$$V(r_o) - V(o) \sim \frac{\mu_o \ell}{2\pi} \dot{I}_o \ell n\, K + \frac{\mu_o \ell}{2\pi} I_o \frac{\dot{K}}{K} .$$

Assuming the pinch ratio is of the order of 3, as it is later seen to be the first term is small compared to $L_E \dot{I}_o$. The second term is correspondingly small averaged over times of interest, since

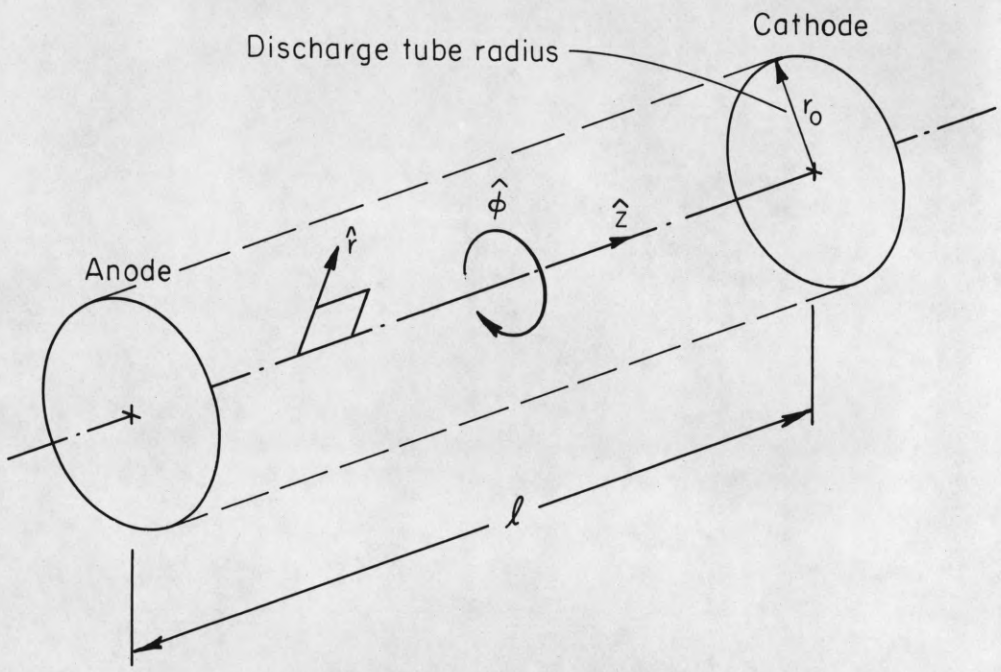

Figure 3.3. Discharge Coordinate System.

$$\frac{\mu_o \ell\ I_o}{2\pi}\ \frac{1}{\Delta t}\int_t^{t+\Delta t}\frac{\dot{K}}{K}\,dt = \frac{\mu_o \ell}{2\pi}\ I_o\ \frac{\Delta\ \ell nK}{\Delta t}$$

$$\lesssim \frac{\mu_o \ell}{2\pi}\ \frac{I_o}{\Delta t}\ \ell nK$$

$$\lesssim \frac{\mu_o \ell}{2\pi}\ \dot{I}_o\ \ell nK$$

for $\Delta t \sim \Omega^{-1}$.

Therefore as long as k is not too large, back emf's inside the tube will not be important in comparison to $L_e\ \dot{I}_o$. We must therefore merely be sure that the secondary current is not too large.

For non-turbulent plasma, the current would only be limited by the speed of light for $E \gg E_c$. However, the plasma will be very turbulent indeed, as it would otherwise be drifting faster than the ion-acoustic velocity, and this turbulence will lower the conductivity.

If the electrons are drifting with the ion-acoustic velocity, then for hydrogen and complete ionitation we have

$$I_o \simeq 6\ A T_e^{\frac{1}{2}} p$$

where A is the tube cross section in cm^2, T_e is the electron temperature in eV, and p is the initial gas pressure in μ-Hg. Then, since $\dot{I}_o \sim \Omega\ I_o$ where Ω is the machine ringing frequency in radians per second, we want

$$L_E\ \Omega\ I_o \sim \alpha\ V_o$$

or

$$I_o \sim \frac{2 \cdot 10^4}{\frac{1}{2} \cdot 10^{-6} \cdot 10^6} = 4 \cdot 10^4 \text{ amperes}$$

using $L_E \sim \frac{1}{2}$ μh, $\Omega \sim 10^6$ sec^{-1}. Then

$$A \sim \frac{4 \cdot 104}{6 \cdot 10 \cdot 100} \sim 6 \text{ cm}^2$$

for p = 100 μ, T = 100 eV.

A 1-inch inside diameter tube was decided upon giving an inside diameter of 5 cm^2. With these tubes the electric field was several hundred volts per cm for pressures of 200 μ for times of interest.

The tubes used were 96% alumina ceramic tubes 16 inches long, 1-inch inside diameter and 1¼-inch outside diameter. The electrodes were machined from stainless steel. The anode had a ¼-inch hole in the center through which diagnostic devices could be inserted, or in which a stainless plug with a small orifice in the center could be placed. This orifice was to allow runaway electrons to escape. The side of the anode away from the discharge was connected via a large manifold to the diffusion pump. The cathode had a 3/8-inch hole in the center which connected the tube with the pre-ionization chamber.

The tube was surrounded by two layers of 0.002-inch shim brass insulated from each other by a thin sheet of mylar. The shim brass sheets had small spiral slits about 1 mm wide to allow the B_z field to pass through. This was wrapped with more thin mylar upon which the B_z coil was wound. This coil consisted of one layer of #24 wire wound close spaced. The return current for this coil was carried by the outer of the two layers of shim brass. The coil was then covered with epoxy and several layers of polyethylene insulation.

The effect of the shim brass was three-fold. It was of such a thickness as to have a decay time of about 5 milliseconds, much longer than all times of interest. It therefore shielded the tube from stray primary fields, tended to maintain the discharge in the center of the tube, thereby increasing the stability of the pinch and helped maintain a uniform B_z field.

3.3 The Condensor Bank

The condensor bank consisted of twelve 2.5 μf fast discharge capacitors. Each of these fired through separate ignitrons to one of the three primary straps in each primary, in the manner that was shown in Fig. 3.2. All of these circuits could have been paralleled, but they fired reliably and reproducibly without it, so the extra complication was unnecessary.

The capacitor bank and firing circuit is shown in Fig. 3.4, and the waveform for the first quarter cycle in Fig. 3.5. Fig. 3.6 shows the thyratron circuit used to fire the trigger ignitron.

3.4 Pre-ionization

Due to the machine configuration pre-ionization was difficult. Radio-frequency breakdown was impractical due to capacitive loading to the B_z coils and shielding. It was difficult to attach a dc electrode in the center and would not work well at low pressures. The method that was adopted was to pulse a discharge at the cathode end of the machine and let the plasma diffuse through a hole in the cathode down the longitudinal magnetic field.

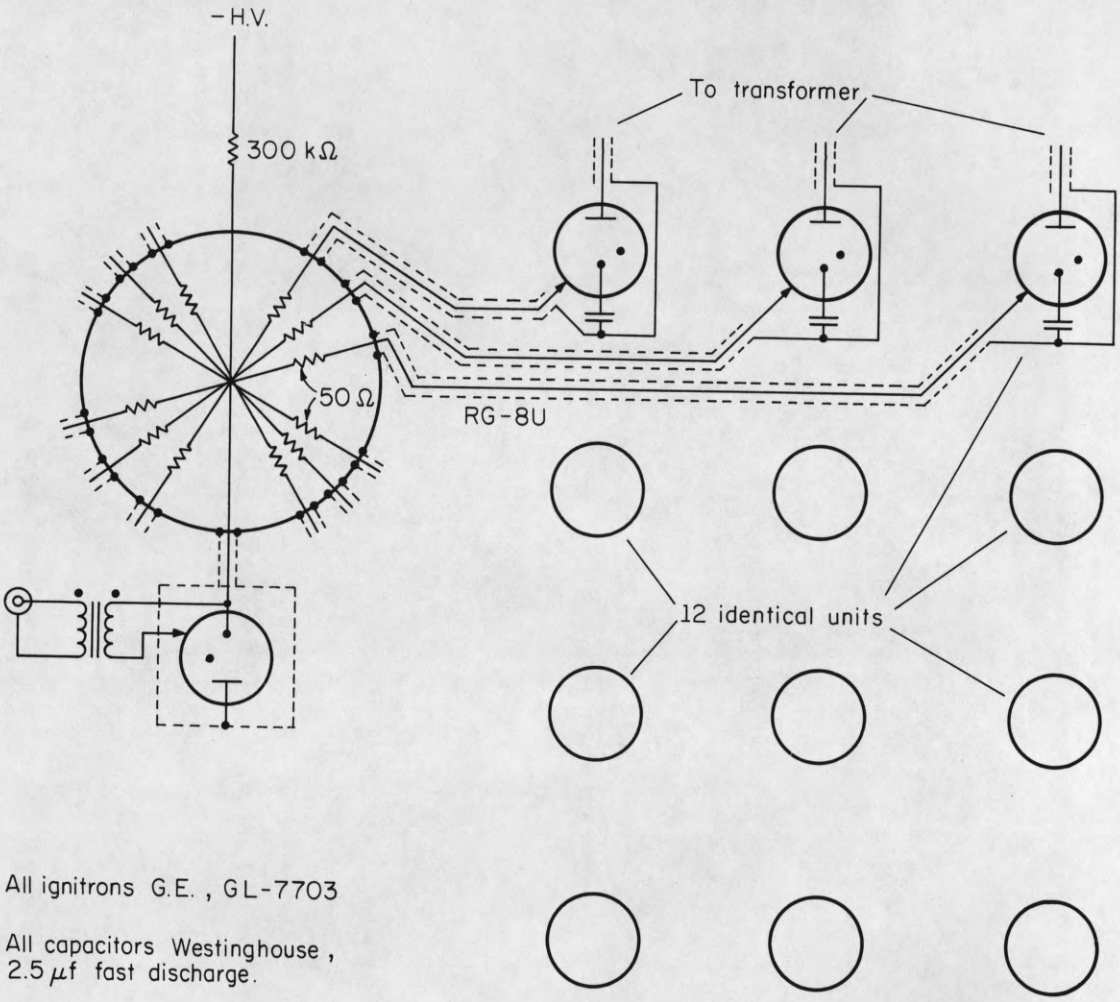

Figure 3.4. Condensor Bank.

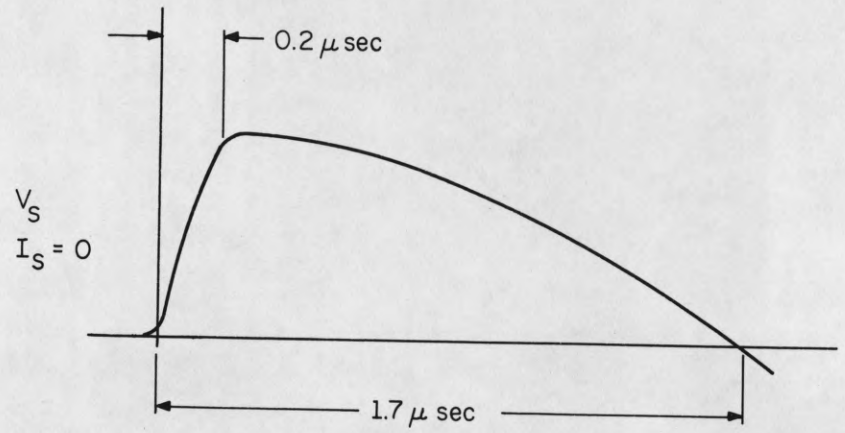

Figure 3.5. Voltage Wave Form First Quarter Cycle.

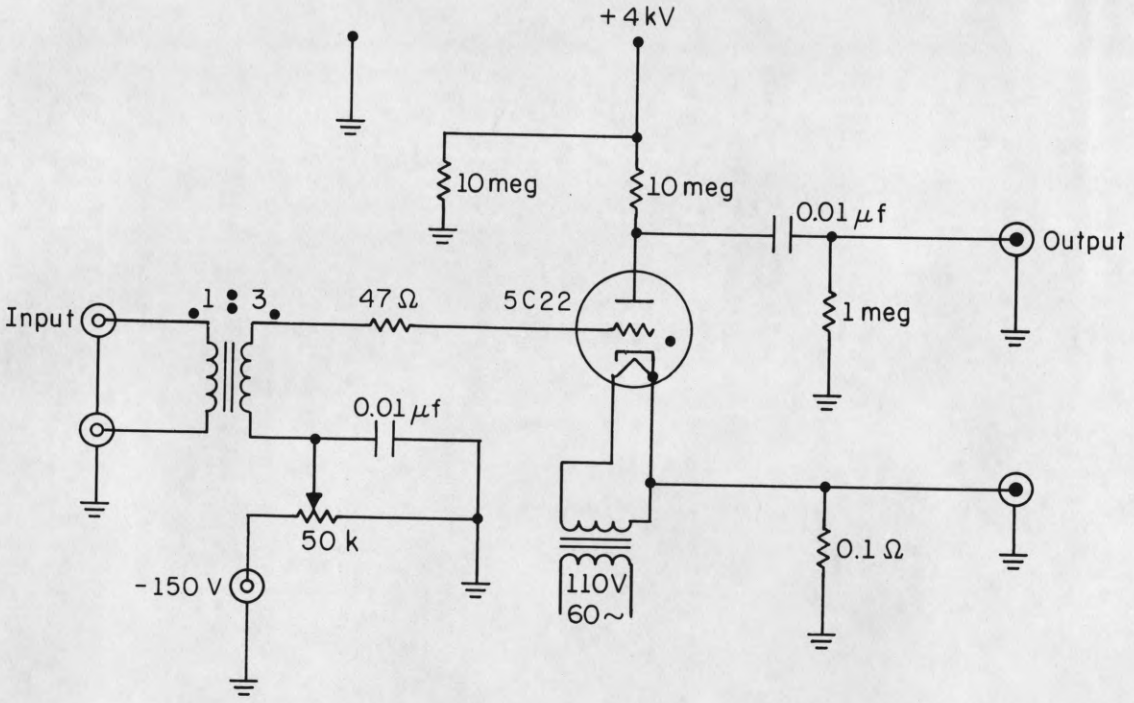

Figure 3.6. Condensor Bank Trigger Circuit.

To get a uniform plasma in the tube the pre-ionizing discharge was pulsed as the longitudinal magnetic field began to build up, and the discharge decayed well before the longitudinal field had reached its peak. Then, when the longitudinal field was near its peak, and approximately constant, the plasma spread and decayed by ambipolar diffusion until the condensor bank fired. Therefore, to have a reasonably uniform plasma down the length of the tube, it was necessary that the diffusion constants normal and parallel to the field obey the relation

$$\frac{D_\perp}{D_{||}} \ll \frac{2a}{\ell}$$

where a is the radius of the tube and ℓ is the length. Assuming $T_e \sim T_i$

$$D_{||} \doteq D_i$$

$$D_\perp \doteq \frac{2D_e}{\Omega_e{}^2\tau^2} = \frac{2D_i}{\Omega_e{}^2\tau^2}\left(\frac{M}{m}\right)^{\frac{1}{2}} = \frac{2}{\Omega_e{}^2\tau^2}\left(\frac{M}{m}\right)^{\frac{1}{2}} D_{||}$$

where $\Omega_e = \frac{eB}{mc}$ and τ is the mean electron-neutral collision time. Then

$$2\left(\frac{M}{m}\right)^{\frac{1}{2}} \frac{1}{\Omega_e{}^2\tau^2} \ll \frac{2a}{\ell}$$

$$\Omega_e{}^2\tau^2 \gg \left(\frac{M}{m}\right)^{\frac{1}{2}} \frac{\ell}{2a} \sim 10^3.$$

Since $\tau = \frac{\lambda}{v_e} = \frac{1}{n_o\sigma_e v_e}$, where n_o is the density of neutrals, σ_e is the elastic collision cross section, v_e is the mean thermal electron

velocity, $\tau \sim \frac{1}{2} \cdot 10^{-7}$ sec assuming $n_o \sim 10^{15}$ cm^{-3}, $\sigma \sim 10^{-15}$ cm^2 and $v_e \sim 2 \cdot 10^7$ cm/sec. For B in gauss $\Omega_e \sim \frac{3}{2} \cdot 10^7 B$ sec^{-1}. Thus $(\Omega_e \tau)^2 \sim B^2 \gg 10^3$, or $B \gg 32$ gauss.

The pre-ionization chamber was a coaxial discharge with a magnetic field provided by the same condensor which fired the discharge. It would work down to pressures of about one micron. Plasma from this chamber passed through a 3/8-inch hole in the cathode and down the B_z field to the other end of the tube. The pre-ionization chamber and firing circuit are shown in Fig. 3.7. The magnet field from the coil around the chamber lowered the minimum operating pressure by increasing the path length of the electrons. The 2K resistor was found to give the lowest possible firing pressure. The system was found to work better with the coil in series with the discharge than parallel to it. The pre-ignition voltage was small compared to 10 kV so that the current decayed with the e-folding time of 10 μsec.

A Langmuir probe at the anode and therefore at the furthest point from the pre-ionization chamber indicated an electron density of 10^{10} to 10^{11} cm^{-3} at the peak in B_z, which was when the condensor bank was fired.

3.5 Ionization

The fact that there was a plasma in the tube when the condensor bank fired did not necessarily mean that the tube would ionize further. For pressures such that the neutral density was above some critical density $n_c \simeq \frac{1}{\sigma_i \ell}$, where σ_i is the ionization cross section

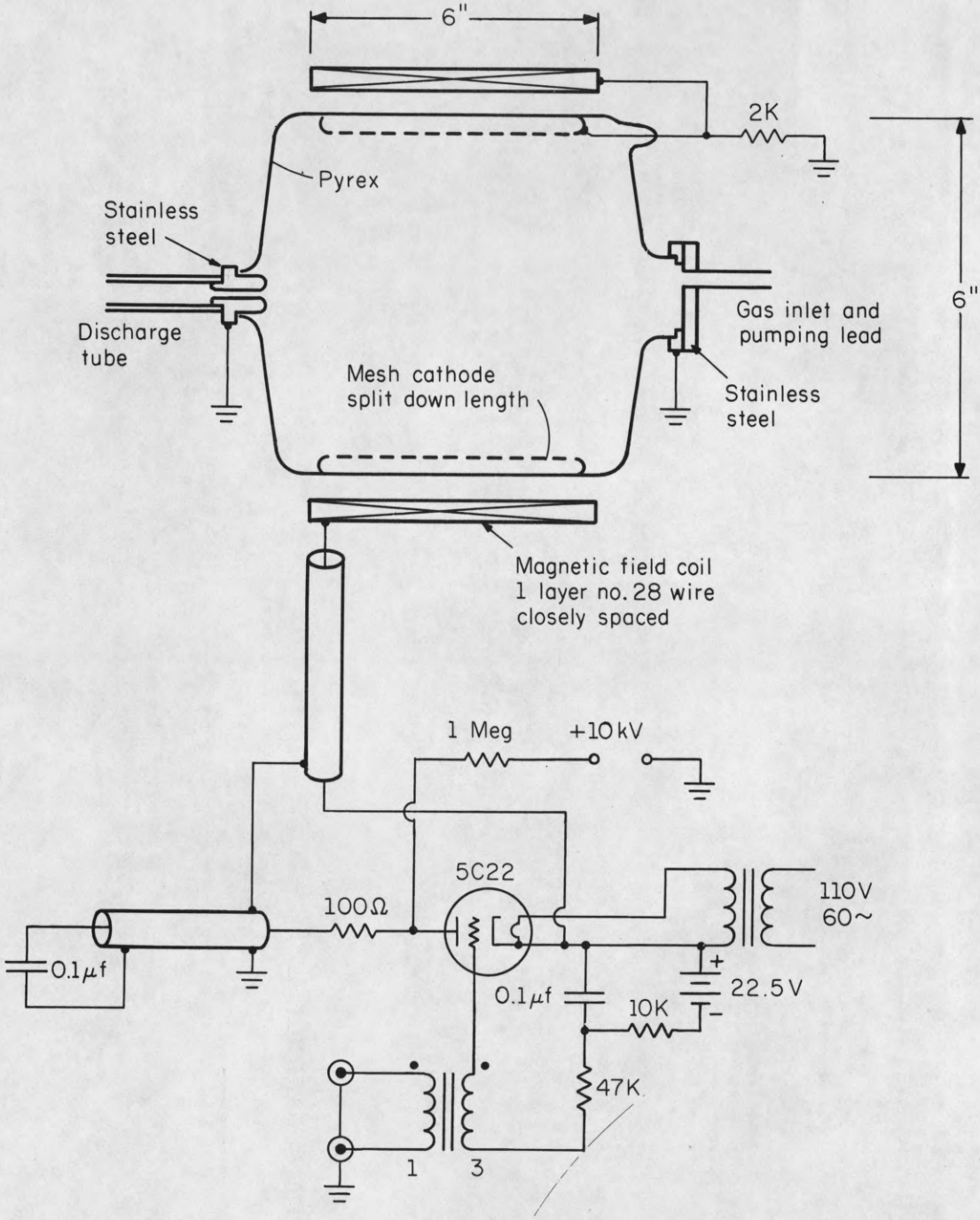

Figure 3.7. Preignition Chamber and Circuit.

and assuming an electron temperature of about 60 eV, it is easily shown that the density e-folding time is about 2/p μsec, when the gas is weakly ionized. Assuming the density must go from 10^{11} cm^{-3} to 10^{16} cm^{-3} this gives an ionization time of about 10/p μsec. Since a ½-μsec delay was all that could be tolerated, p had to be greater than about 20 μ. Actually, the delay was ½ μsec at about 30 μ.

3.6 Longitudinal Magnetic Field

The longitudinal magnetic field was produced by discharging a 10 μf capacitor charged to 1400 volts through the coil around the discharge tube. While lower fields could have been used, the best results were obtained at the highest possible field. The discharging circuit is shown in Fig. 3.8.

The coil around the tube was wound at 18 turns per cm, or 23 gauss per amp for a coil in free space. However, the transformer around the coil changes the field. The situation is essentially that seen in Fig. 3.9. The total flux through the machine will be constant (zero) over times of interest. Therefore,

$$\pi B_o(b^2 - a^2) = B_i a^2$$

and

$$B_i + B_o = \mu_o NI$$

so

$$B_i/I = \mu_o N\left(1 - \frac{a^2}{b^2}\right) = \mu_o N(0.31) = 7.1 \text{ gauss/amp} .$$

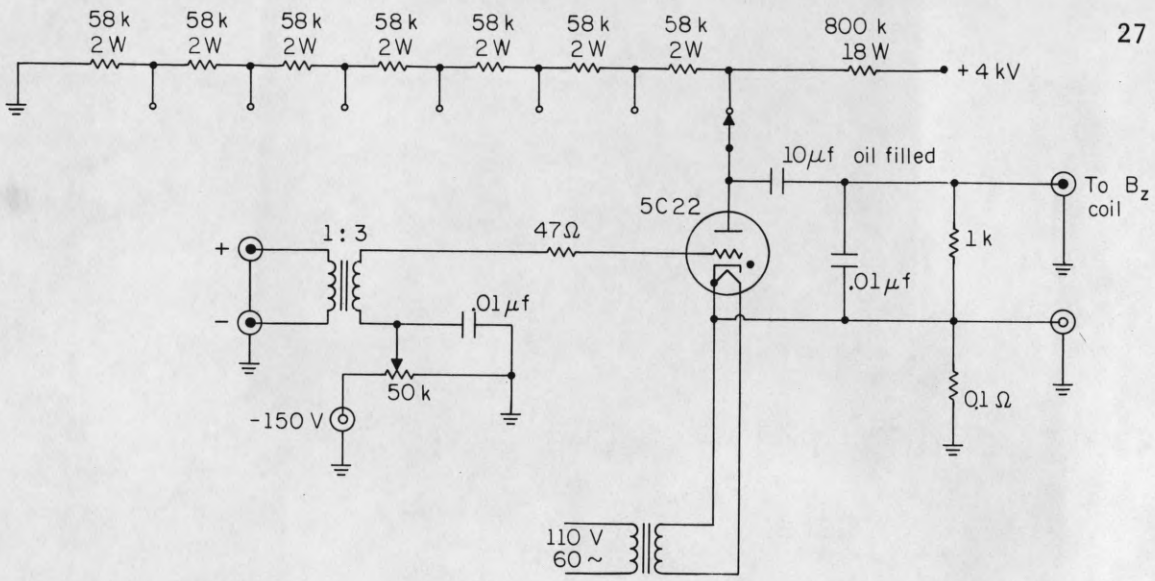

Figure 3.8. Longitudinal Magnetic Field Circuit.

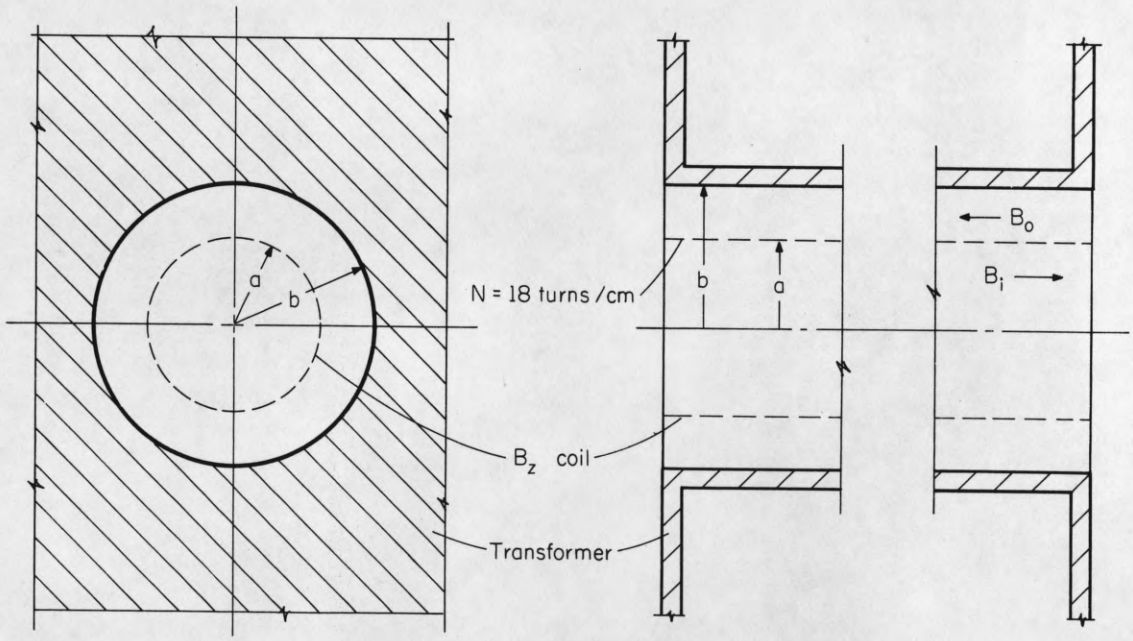

Figure 3.9. Longitudinal Field Coil.

The peak value of I, where the condensor bank was fired, was 75 amps, giving a B_z of 530 gauss.

3.7 Vacuum System

Since high currents were to be drawn from metal electrodes, impurity level was high and a high vacuum was of little use. No particular efforts were made beyond eliminating all leaks, for this reason. The schematic of the system is shown in Fig. 3.10.

A 4-inch, metal, water cooled, oil diffusion pump was used. It was connected via a manifold to the system at the anode end of the machine. The pressure at machine, as measured by the Bayard-Alpert gauge in Fig. 3.10 was below 10^{-6} Torr when no gas was being let into the system. When hydrogen was being admitted the pressure on the manifold side of the anode was below 10^{-5} Torr for a pressure of 0.2 Torr (200 μ-Hg) in the discharge tube. The walls of the tube emitted large amounts of gas when the machine was first fired after being let up to air. This disappeared after a few firings.

Since this was a flowing system working well below the gas supply pressure, the pressure had to be controlled continuously. This was accomplished with a Phillips-Granville controlled variable leak arranged to keep the ion current of a Westinghouse 7903 high pressure ion gauge constant. The electron current was regulated by an automatic filament supply. Regulation was within a few percent.

The high pressure ion-gauge calibration was checked against a Pirani gauge. The agreement was very good throughout the range of interest.

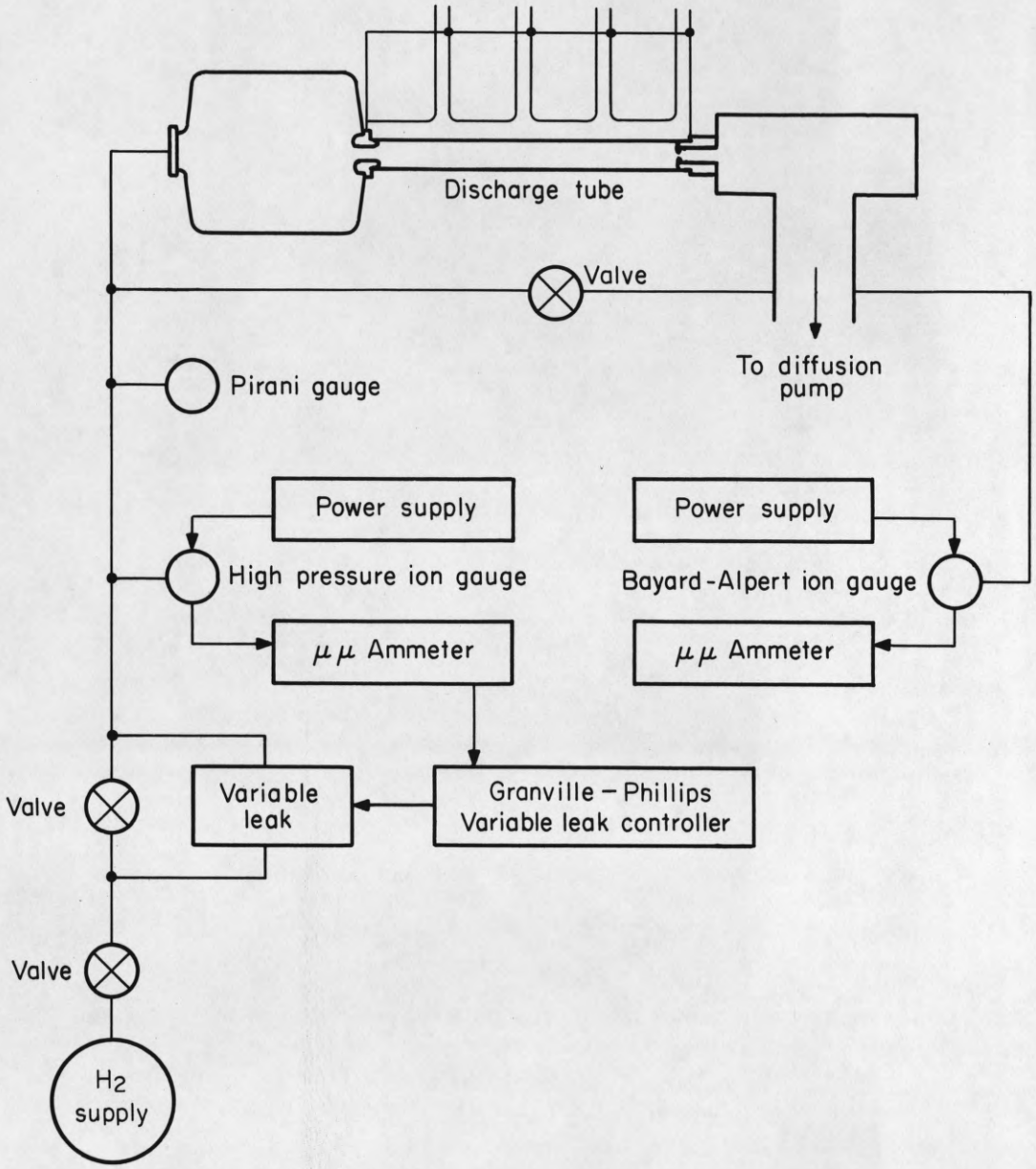

Figure 3.10. Vacuum System.

The hydrogen supply was a one liter static bottle which was filled to about 100 Torr from a high pressure hydrogen tank. Again there was no reason to try for purity.

3.8 Oscilloscope Connections

The cables taking the signals to the oscilloscope were all RG-8U coaxial cable. The impedance was 50 ohms and was matched whenever it was necessary. All cables were grounded to a brass plate near the oscilloscope. Ground currents through the oscilloscope were avoided this was as they were found to cause appreciable deflections.

Noise from the machine was understandably large, but only showed up on the oscilloscope at large gains, with the exception of certain experiments where ground loops were necessary.

The oscilloscope was triggered by a small loop in one of the primaries of the machine.

The conduction current was measured by a Rogowski belt and integrator. The signal went to the oscilloscope through one of the coaxial cables, and the cable was matched at the oscilloscope end. A simple RC integrator was placed at the input of the oscilloscope. The relation between the conduction current and the oscilloscope voltage is

$$I = \frac{t}{M} V$$

where I is the current, t is the integration time constant, M is the mutual inductance to the conductor through the Rogowski belt, and V is the output voltage. The frequency response is limited at both high and low frequencies by

$$\omega_\ell \ll \omega \ll \omega_h$$

where

$$\omega_\ell t = 1$$

and

$$\frac{\omega_h L}{R_o} \simeq \frac{\omega_h NM}{R_o} = 1$$

in which L is the self inductance of the Rogowski belt and R_o is the coaxial cable impedance. L is approximately NM where N is the number of turns of wire on the belt.

For the Rogowski belt we used $\omega_\ell \lesssim 0.1\ \mu sec^{-1}$ depending on the integrator used, and $\omega_h \simeq 210\ \mu sec^{-1}$. Since $\omega \gtrsim 1\ \mu sec^{-1}$ was of interest the low frequency condition was always met, and there was a large range into high frequencies.

M = 17.6 mμh for our Rogowski belt gave values of t/M on the order of 1 kiloampere per volt for the integrators we used.

3.9 Machine Parameters

The values of L_p, L_s, and M were measured. L_p was obtained from the ringing frequency for $I_s = 0$ and the known value of C. The ratio of secondary to primary voltage then gave M. L_s could be and was obtained by measuring the ringing frequency for $V_s = 0$ (a brass pipe the size of the inside of the tube was used as a short) but this involves taking the difference between similar measured quantities and was not very accurate. A more accurate method was used to measure the secondary current for $V_s = 0$. This value of L_s was used and differed from the other by about 12%.

Figure 3.11 shows the equivalent circuit, the measured values of the parameters, and the equations of the machine.

The actual circuit is shown in Fig. 3.12. In this circuit the difference between $\frac{1}{4} L_p$ and $\frac{1}{4} M$ is made up of the inductance of the condensors, ignitrons, and coaxial cables for three units in parallel.

3.10 Experimental Arrangement

Figure 3.13 shows a block diagram of the experiment. The upper trace of the oscilloscope (U) went to the particular experiment being done. This will be discussed in connection with the data.

The delay generators shown are Telectronics type 200AA's. These were adjusted to give the sequence of events seen in the figure.

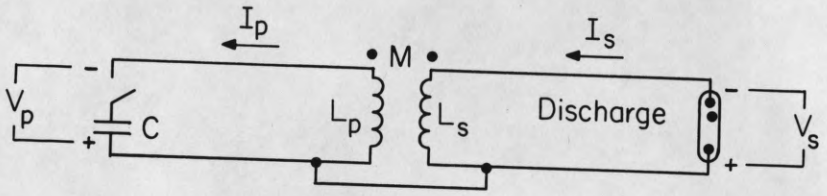

$$L_p C \ddot{V}_p + V_p = -M \dot{I}_s$$

$$V_s = -MC\ddot{V}_p - L_s \dot{I}_s$$

$$= \alpha V_p - L_E \dot{I}_s$$

$$V_s = \alpha V_o \cos \Omega t - L_E \dot{I}_s - \frac{M^2}{L_p^2 C} \int_o^t I_s(t') \cos \Omega(t-t')\, dt'$$

$$= 0.52 V_o \cos 0.98t - 0.36 \dot{I}_s - 0.15 \int_o^t I_s(t) \cos 0.98(t-t')\, dt'$$

for volts, amperes and μs or kilovolts, kiloamperes, and μs.

$V_o = 4V_c$ where V_c is the condenser bank voltage.

$C = 1.875\ \mu f$

$L_p = 0.56\ \mu h$

$L_s = 0.30\ \mu h$

$M = 0.51\ \mu h$

$$L_E \equiv L_s - \frac{M^2}{L_p} = 0.36\ \mu h$$

$$\alpha \equiv \frac{M}{L_p} = 0.52$$

$$\Omega \equiv \frac{1}{\sqrt{L_p C}} = 0.98\ \mu s^{-1}$$

Figure 3.11. Machine Equivalent Circuit and Parameters.

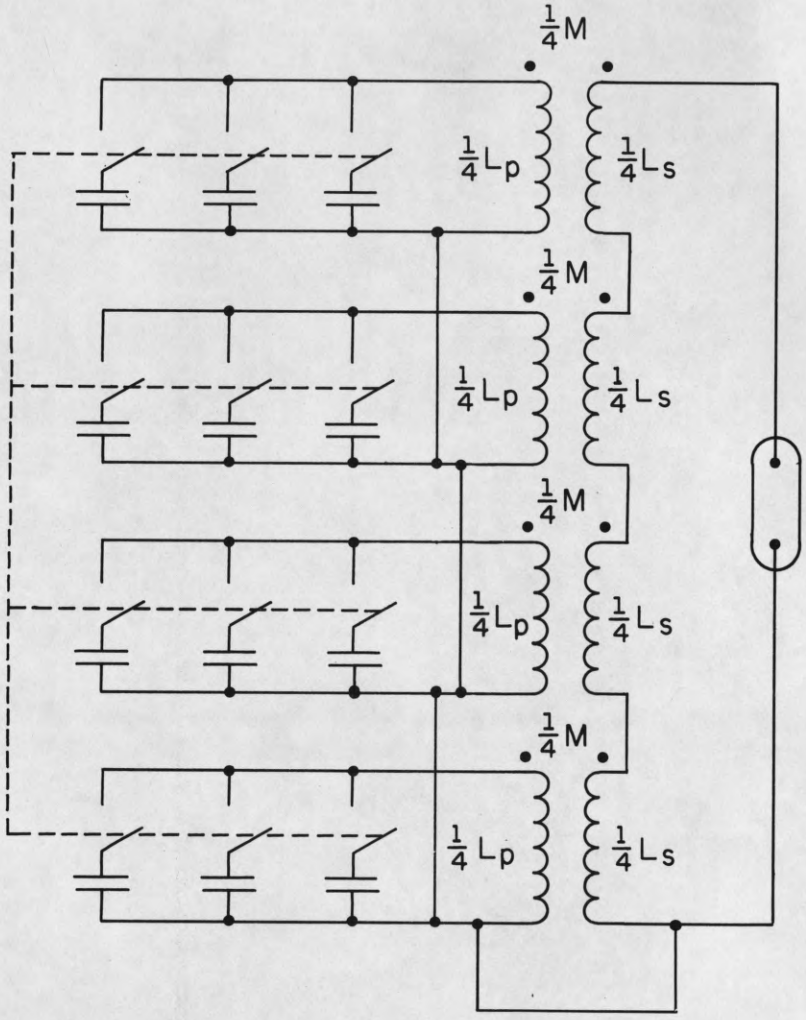

Figure 3.12. Machine Actual Circuit.

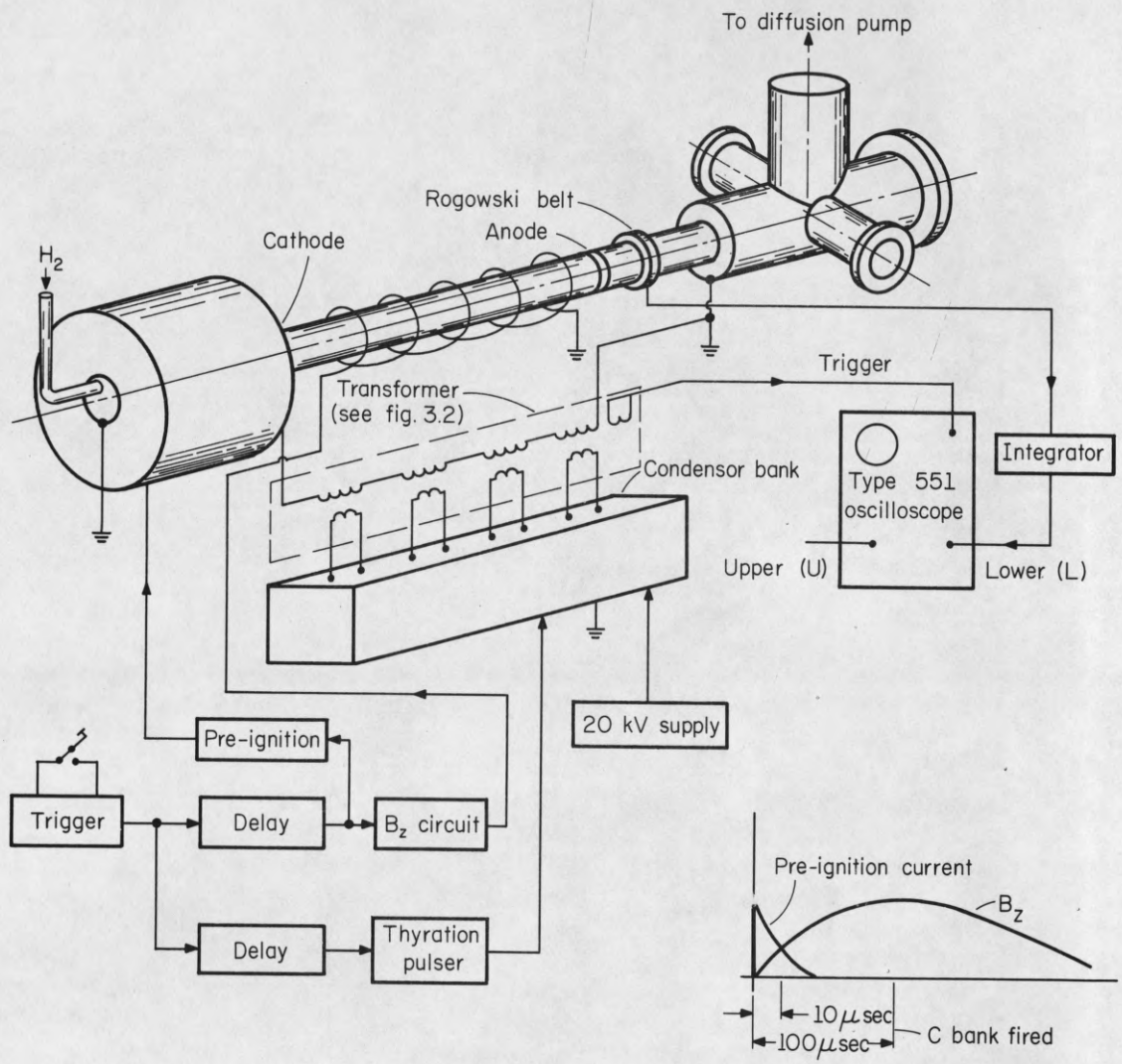

Figure 3.13. Block Diagram of Experiment.

4. Measurements

The application of diagnostic techniques met with a variety of difficulties. To begin with, the plasma was quite inaccessible, being in the center of the transformer. In addition, temperatures, densities, and frequencies were high and the repetition rate was low.

All experiments were recorded on 3000 speed Polaroid film from a Tektronics type 511 dual beam oscilloscope. Since the condensor bank time constant was 12 · 2.5 μf · 0.3 megohms = 9 seconds, it was necessary to wait at least 45 seconds between successive experiments while the condensor bank voltage built up.

In each of the experiments the oscilloscope was triggered from a pickup loop in one of the primaries. The scope triggered very early in the rise time. The lower oscilloscope trace was always the conduction current, taken from the Rogowski belt, so that results could be compared and reproducibility checked.

4.1 Runaway Electrons

The approximate energy of the runaway electrons was obtained by looking at the absorption of bremstrahlung from a tungsten target by thin aluminum sheets. The electrons passed through a 0.030-inch hole in the center of the anode to a tungsten target about 6 inches away. The experimental setup is shown in Fig. 4.1. The scintillator received many X-rays on each pulse, so the photomultiplier current was high ($\sim$ 1 milliamp) and background noise posed no problem. A typical oscilloscope trace is shown in Fig. 4.2.

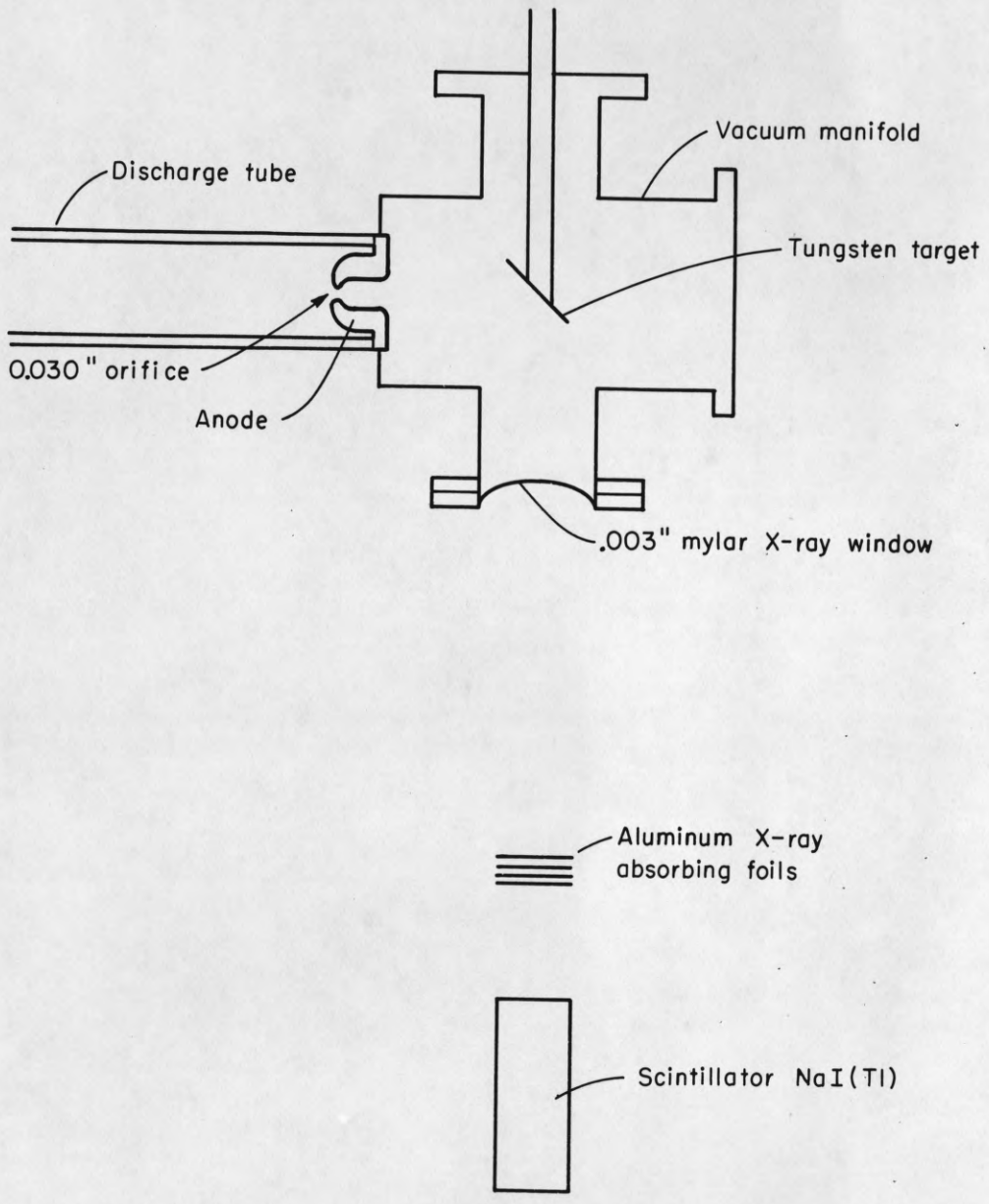

Figure 4.1. Runaway Electron Energy Experimental Arrangement.

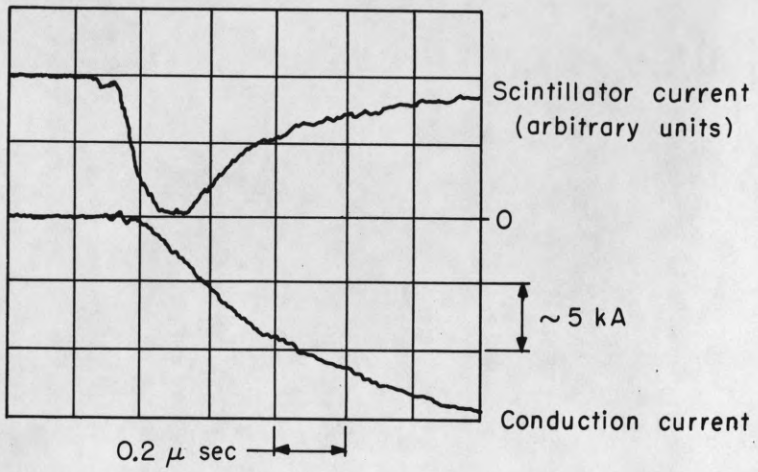

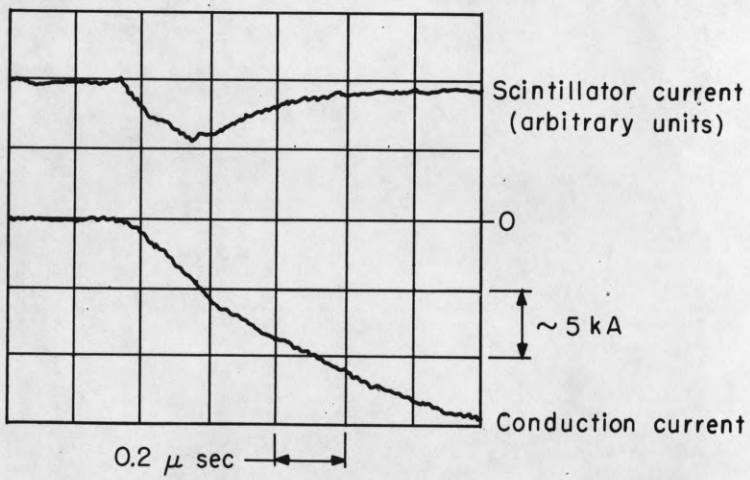

Figure 4.2. Scintillator Response for No Absorber and 0.008 inch Al Absorber.

Figure 4.3 shows a plot of pulse height versus absorber thickness. This was obtained from the oscilloscope trace from the scintillator with various numbers of 0.001-inch thick aluminum absorbers between the target and the scintillator. The scatter shown is typical. These plots all indicated energies in the 10 keV range. This is roughly equal to the voltage down the tube.

The slightly later peak in the scintillator current (Fig. 4.2) for thick absorber was always found. Since the runaway current is decreasing rapidly at this time, it implies that the average runaway electron energy is higher at this later time. This may be due to fewer collisions with neutrals.

Figure 4.4 is a plot of the pulse height versus condensor bank voltage for a constant pressure and abosrber thickness. Each point is the average of a few firings.

The runaway current of the electrons was measured by a collector on the manifold side of the anode, Fig. 4.5. It was designed in such a way as to avoid secondary currents and photo currents. Applying a stopping voltage on the collector had no noticeable effect for stopping voltages less than 1 kV. Moving the collector to one side also had little effect. This implies that the beam is spread at several degrees from the tube axis. Figure 4.6 is an oscilloscope trace of the runaway current and conduction current for a particular set of parameters. The oscillations in the latter part of the runaway current are due to a necessary ground loop causing some of the conduction current trace to appear.

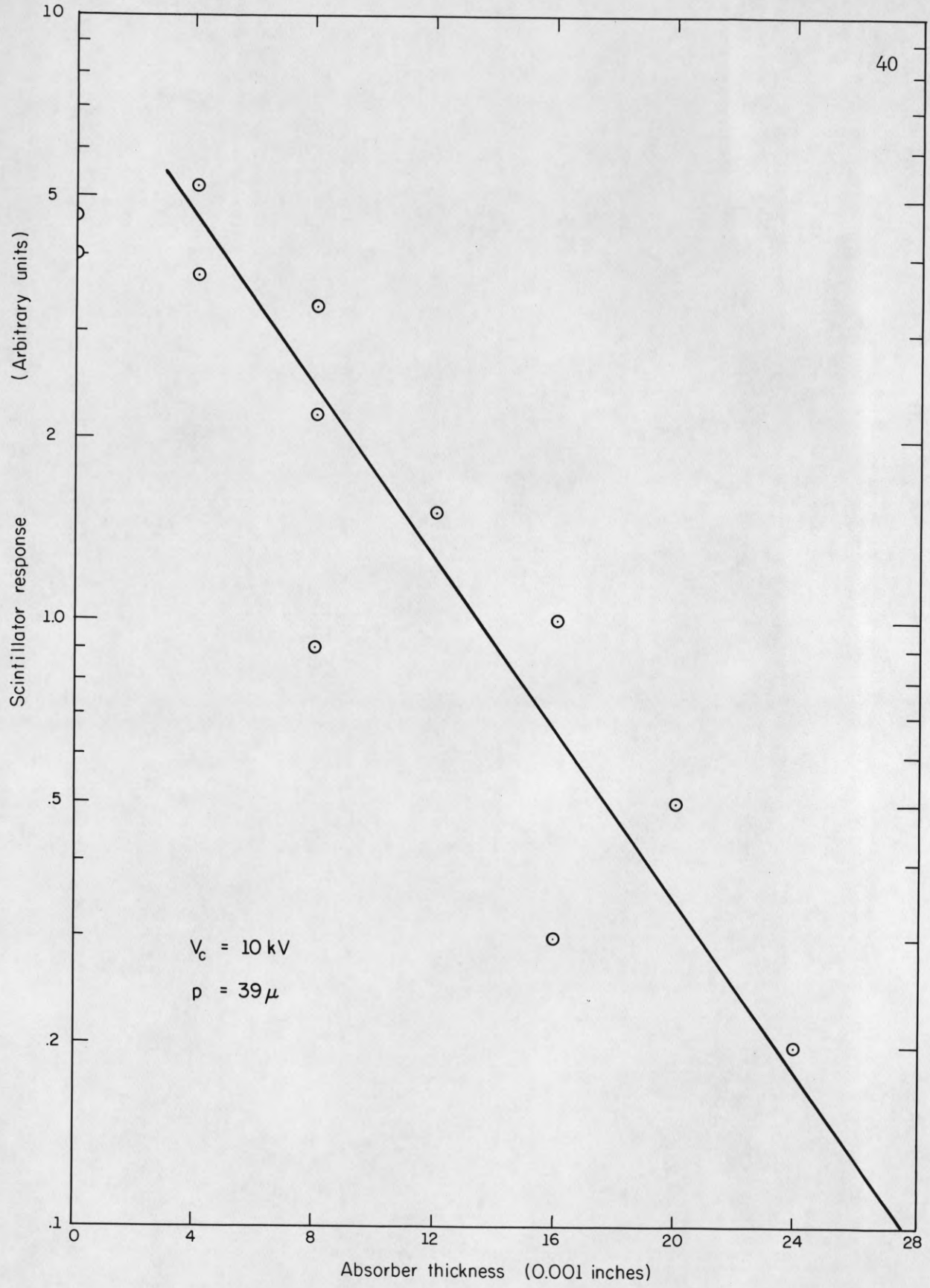

Figure 4.3. Pulse Height versus X-ray Absorber Thickness for a Typical Electron Energy Experiment.

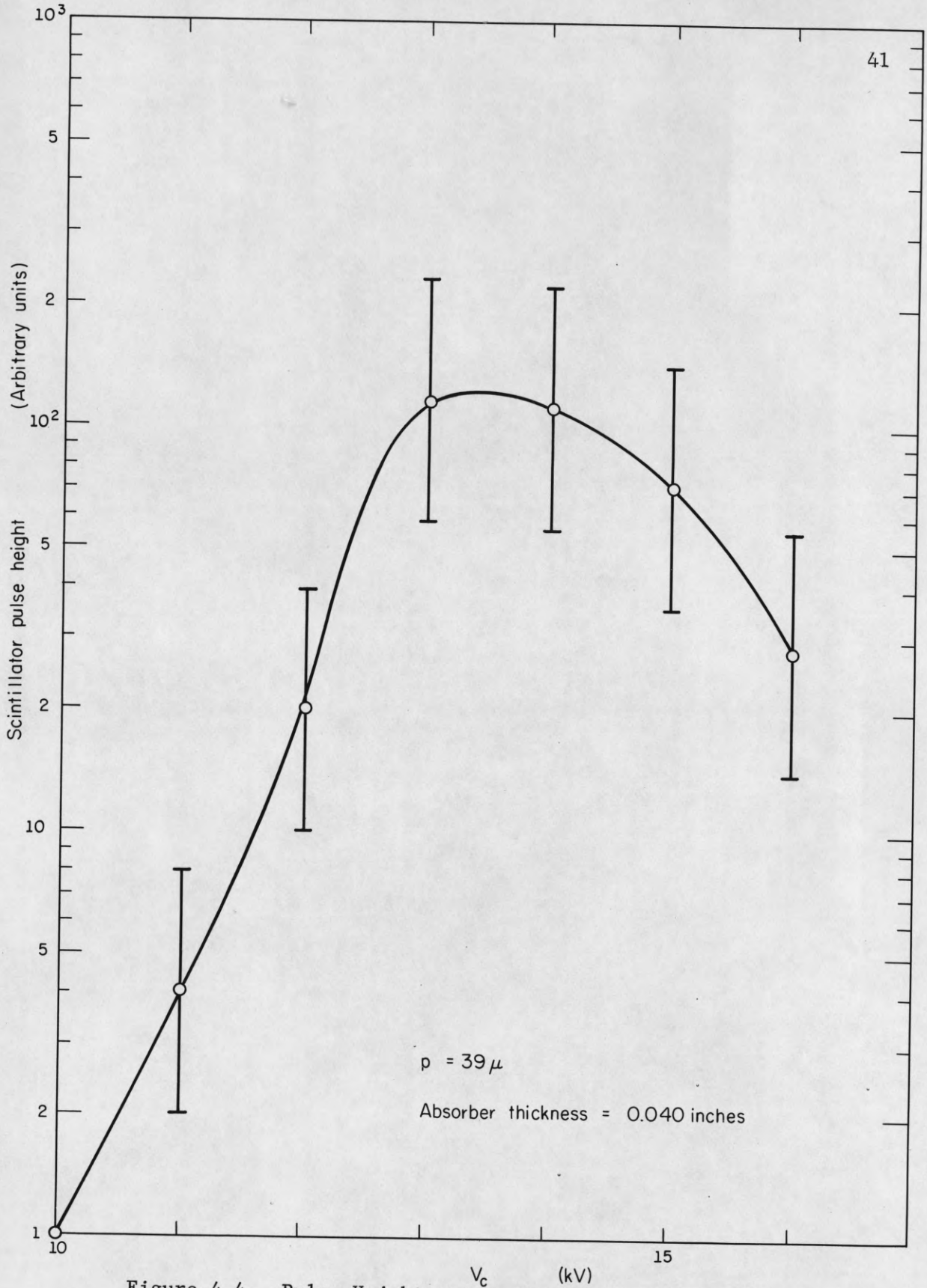

Figure 4.4. Pulse Height versus Condensor Bank Voltage, V_c, for Constant Pressure and Absorber Thickness.

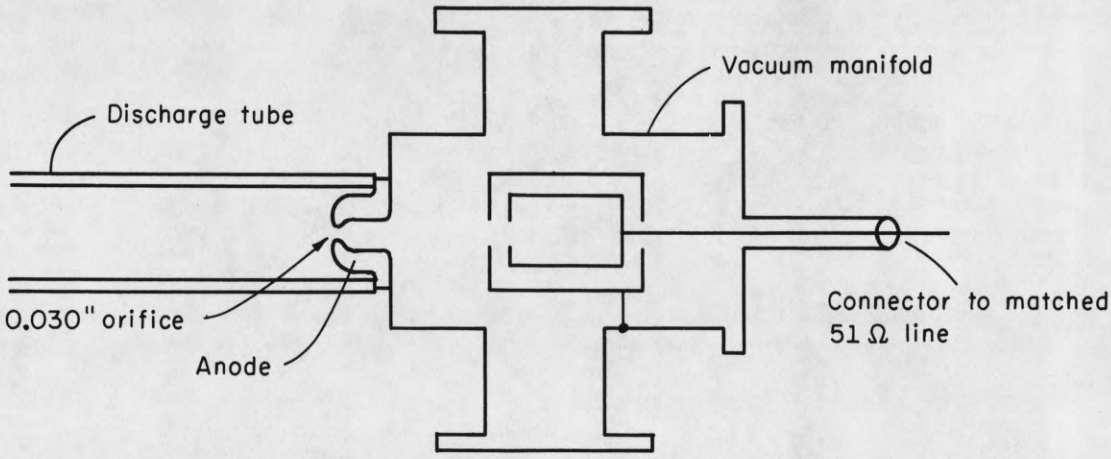

Figure 4.5. Runaway Current Experimental Arrangement.

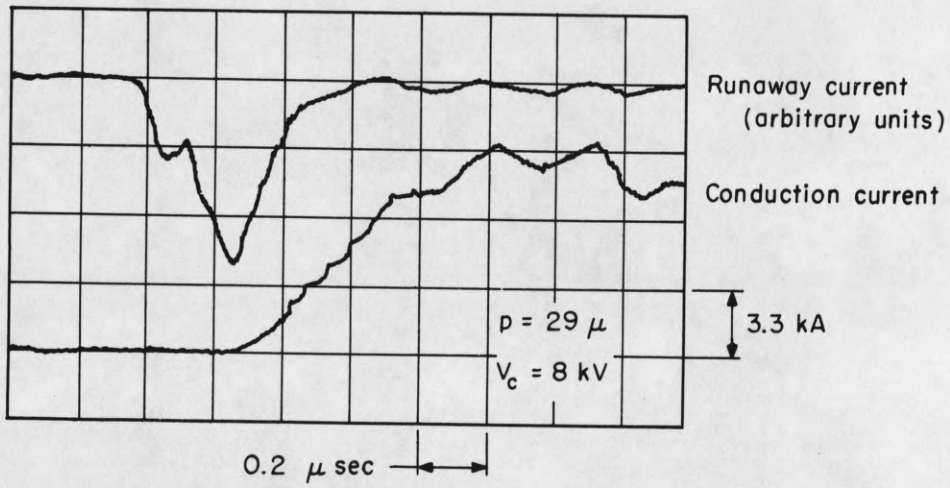

Figure 4.6. Typical Runaway Current Oscilloscope Trace.

The currents measured were in the milliampere range and when divided by the area of the orifice through which they passed amounted to the order of amps per cm^2. This is down by 10^4 from the conduction current densities. However, the probe measurements which will be mentioned later indicated that there were pulses of high energy electrons with currents of kiloamperes per cm^2 during runaway. The discrepancy can be explained by the fact that the collector only collects electrons moving at small angles to the axis of the tube. The fast electrons may be deflected through small angles by collisions and the beam will be spread additionally by passing through the sheath which must bulge into the orifice in the anode, thus becoming a lens for charged particles. Since the electron temperature does not vary much in this experiment (as will be shown later) and the orifice does not change, the voltage across the lens (sheath) and the curvature are approximately constant. We will therefore assume the total runaway current is proportional to the collector current.

Figure 4.7 shows a plot of the peak runaway current versus pressure for several condensor bank voltages. Several interesting things are found. One is that the current at low pressure does not depend strongly upon condensor bank voltage. This, in conjunction with Fig. 4.4 indicates that the runaway energy is peaked at around V_c = 13.5 kV. Another unexpected result is that the peak runaway current drops off more rapidly with pressure at 14 and 16 kV than at lower condensor bank voltages. A possible explanation for these two facts might be that the density is higher at the high condensor bank

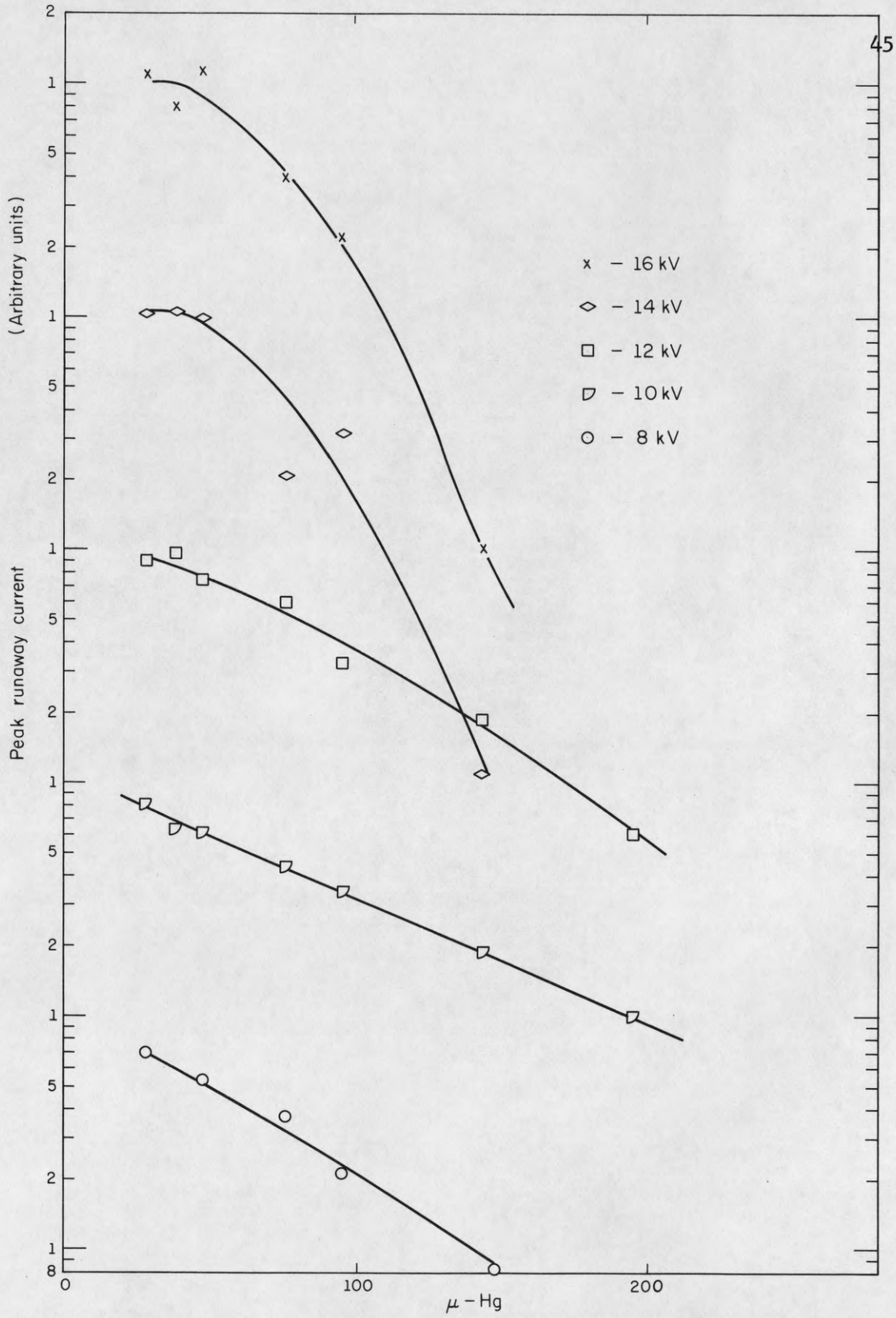

Figure 4.7. Peak Runaway Current versus Initial Gas Pressure. There is a one decade shift in current between curves for different condensor bank voltages.

voltage due to higher pinch ratios and, at higher pressures, due to more complete ionization.

It will be shown in a later section that the electric field is greater than the critical electric field due to ions and neutrals for the complete range of parameters investigated here. In spite of this, runaway always disappeared in a few tenths of a microsecond after the conduction current became large.

4.2 Current Profiles and Electric Field

Because of the high electric fields and high current densities rapid ionization and density changes occur in the plasma. Our requirement of a thick sheath so that the electric field along the axis is high also means that the B_z field diffuses rapidly, and that a rapidly moving pinch may occur. This pinch cannot be considered with the snowplow model, however, due to the thick sheath. Instead, as the gas is ionized the ions and electrons are moved toward the center. The high resistance due to collisions with neutrals permits the plasma and magnetic field lines to move with respect to each other.

A probe for measuring the magnetic field in the θ-direction was built and placed in one of the discharge tubes. It was manipulated from the cathode end (through which it passed) and could be moved to different radii (Fig. 4.8). Due to the method of changing the position of the probe, the cosine of the angle between the normal to the coil and B_ϕ had to be taken into account. In addition, because of the way the probe was constructed, it was not possible to prevent

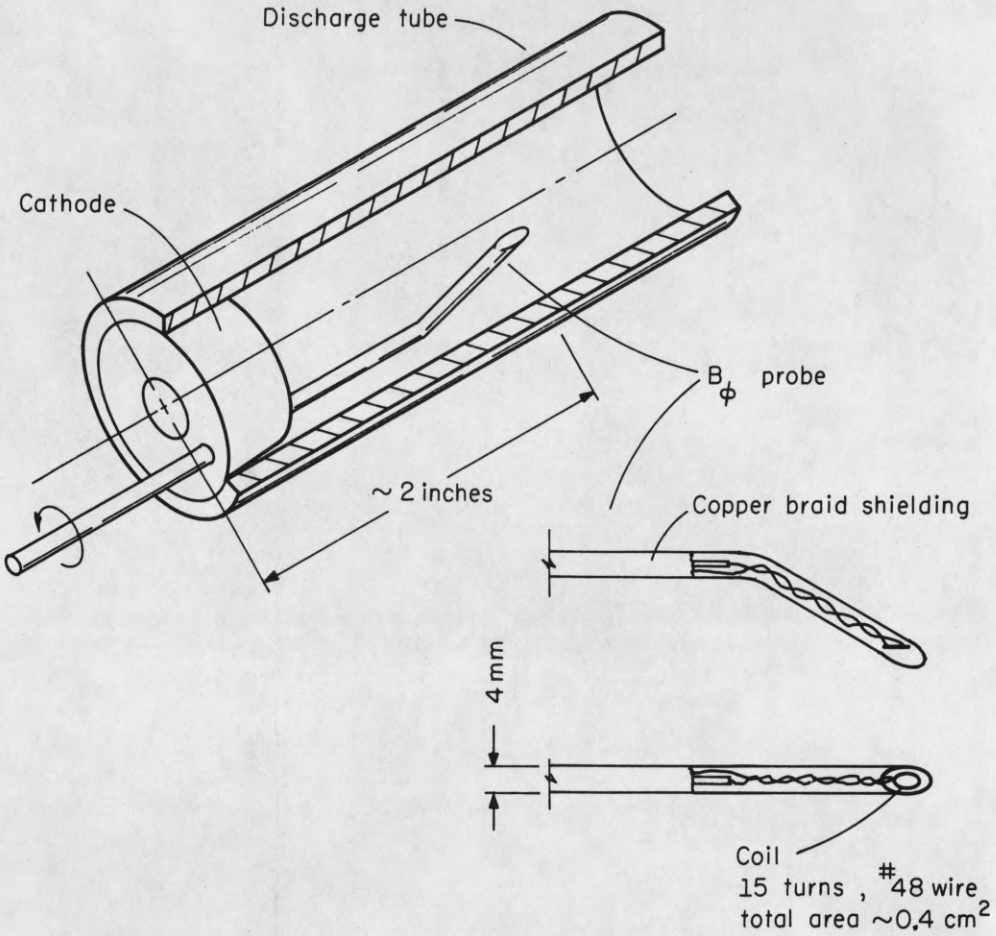

Figure 4.8. Magnetic Probe Experimental Arrangement.

the probe from seeing a small component of the changes in B_z. By putting the probe at two different positions with the same radius this effect could be cancelled. It was also possible to get B_z as a function of the time this way, but it was so error-prone, due to the fact that it involved taking the difference between two similar oscilloscope traces, that it was not done.

The smallest probe we were able to build was made of 4 mm pyrex tube with a 1.5 mm coil inside. This probe was not much smaller than typical pinch radii and therefore undoubtably disturbed the plasma when it was near the axis of the tube. It also would not have been very useful to move the probe in small increments compared to 4 mm. We therefore used the probe to get the conduction current inside of r = 0.3 cm (I(0.3)) and inside of r = 0.6 cm (I(0.6)). We found no reason for considering larger r as most of the current was inside of r = 0.6 cm for times of interest as shown by comparison of I(0.6) and I_o, the current measured by the Rogowski belt. A few firings were tried at larger radii to confirm this.

The currents displayed on the oscilloscope were quite reproducible except for oscillations of about 10% of the trace. The oscillations appeared a few tenths of a microsecond after the current began to rise. These oscillations were averaged to get I(r). The source of these oscillations will be discussed later.

Equation (3.5) gives the integral of the electric field down the axis of the tube. Writing this as an average of the electric field down the tube

$$\ell E(o) - V(r_o) = V(o) - V(r_o) = \frac{\mu_o \ell}{2\pi} \frac{d}{dt} \int_o^{r_o} \frac{I(r)}{r}\, dr.$$

Since $V(r_o) = V_s$ and $I_o = I_s$, combining this with Eq. (3.4) yields

$$\ell E(o) = \alpha V_o \cos\Omega t - L_E \dot{I}_o - \frac{M^2}{L_p {}^2 c} \int_o^t I_o(t') \cos\Omega(t-t')\, dt'$$

$$- \frac{\mu_o \ell}{2\pi} \frac{d}{dt} \int_o^{r_o} \frac{I(r)}{r}\, dr \ .$$

The third term on the right is due to the effect of the secondary current changing the primary voltage. By assuming I_o behaves as seen in the following sketch

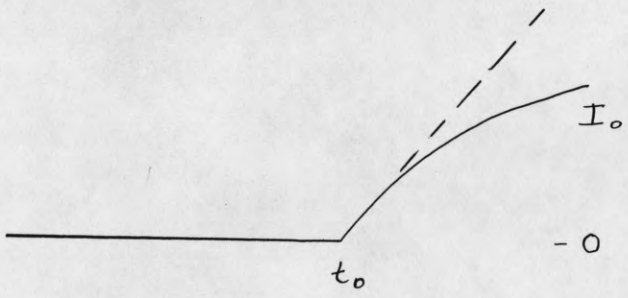

it is easily shown that this term is less than

$$\alpha^2 L_p \left.\frac{dI_o}{dt}\right|_{t-t_o} \frac{[\Omega(t-t_o)]^2}{2}$$

or about

$$0.2\, [\Omega(t-t_o)]^2$$

times the second term. We will only be interested in $\Omega(t-t_o) \lesssim 0.7$ so this term is down by a factor of 10 from the second term and will be neglected.

The fourth term on the right may be written as

$$L_o \frac{d}{dt} (I_o F)$$

where $L_o = \frac{\mu_o \ell}{2\pi} = 0.008\ \mu h$ and F is a function only of the shape of the current distribution.

$$F = \frac{1}{I_o} \int_o^{r_o} \frac{I(r)}{r}\, dr$$

As mentioned earlier this has a value of approximately ln K for any reasonable pinch distribution of pinch ratio K. For example, for a Bennett distribution

$$j(r) = \frac{\text{constant}}{\left[1 + \left(\frac{1}{K}\right)^2\right]^2}$$

$$F = \frac{1}{1 + \frac{1}{K^2}} \frac{1}{2} \ln (1 + K^2) = \ln K + \sim \left(\frac{1}{K^2}\right) .$$

In this machine ln K is roughly one. For that reason the expression we use for the electric field is

$$\begin{aligned} \ell E(o) &= \alpha V_o \cos\Omega t - (L_E + L_o)\, \dot{I}_o \\ &= 0.52\, V_o \cos 0.98t - 0.44\, \dot{I}_o \end{aligned} \tag{4.1}$$

with V_o in volts, t in microseconds, and I_o in amperes.

Since the current is not appreciable for times less than t_o we will measure time from that point. Equation (4.1) may then be written

$$\ell E(o) = 0.52\ V_o \cos\Omega(t_o + \tau) - 0.44\ \dot{I}_o \qquad (4.2)$$

$$V_o = 4V_c$$

where V_c = condensor bank voltage, and τ is the time after t_o as seen in the following drawing.

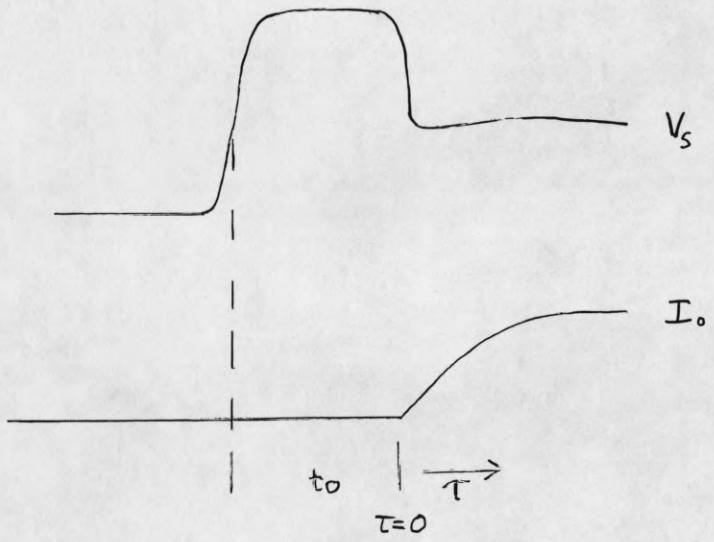

The conduction current I_o often has oscillations of period of about 0.2 μs (cf. Fig. 4.6) as opposed to the 6 μs period of the machine. Because of their high frequency they would have an appreciable effect when put into Eq. (4.2). However, the skin effect would average these out for the field along the axis. For this reason, a smooth line was drawn through these in obtaining the electric field.

Figures 4.9 and 4.10 show graphs of the conduction current and electric field versus time for a low and a high pressure. The condensor bank voltage is 8 kV for both figures. It is seen that at high pressure almost all of the current is inside of r = 0.6 cm, whereas at low pressure this is not true, except for very early times. As condensor bank voltage was raised, the time at which I_o and I(0.6) parted became earlier.

This behavior can be understood as follows. The resistivity due to collisions with neutrals is

$$\eta_o = \frac{m_e v_e}{n_e e^2 \lambda_{eo}} = \frac{m_e v_e \sigma_{eo}}{e^2} \frac{n_o}{n_e}$$

$$\eta_o \simeq \frac{1}{2} \cdot 10^{-4} T^{\frac{1}{2}} \simeq \frac{2}{3} \cdot 10^{-3} \frac{n_o}{n_e} \Omega\text{-cm}$$

for 200 eV electrons. Electron-ion collisions have been neglected here as being unimportant as can be seen from Eq. (2.3). The time for electrons to diffuse across field lines (or field lines to diffuse through the electrons) is then

$$t = \frac{\mu_o a^2}{\eta_o} \simeq 0.2 \frac{n_e}{n_o} \quad [\mu \text{ sec}] .$$

Therefore, at small ionization fraction $\frac{n_e}{n_o}$, the electrons can move toward the center without increasing the magnetic pressure due to B_z.

At high pressures (above about 100 μ-Hg) the ionization never approaches 100% in the first quarter cycle.

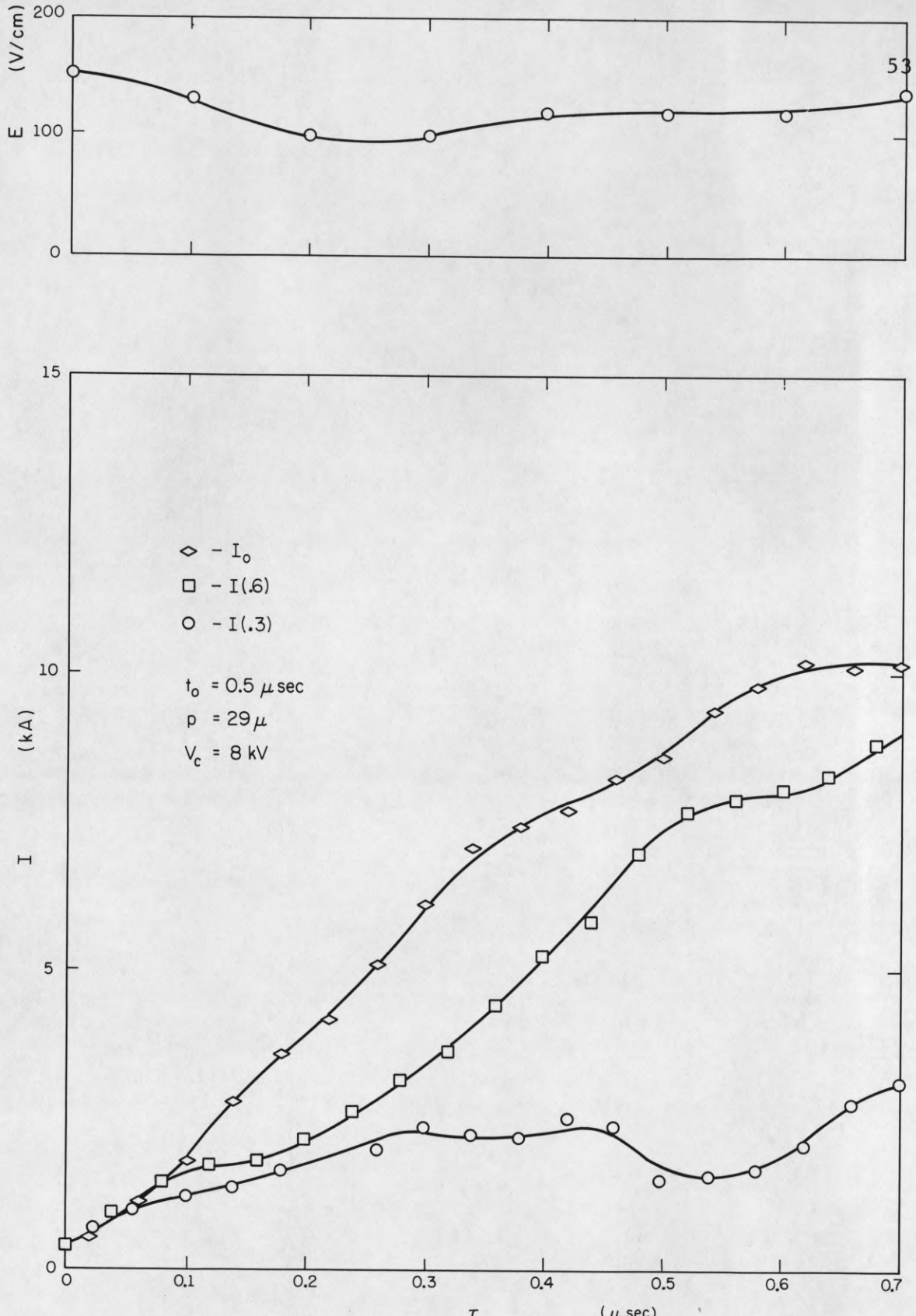

Figure 4.9. Conduction Current and Electric Field at a Low Initial Gas Pressure.

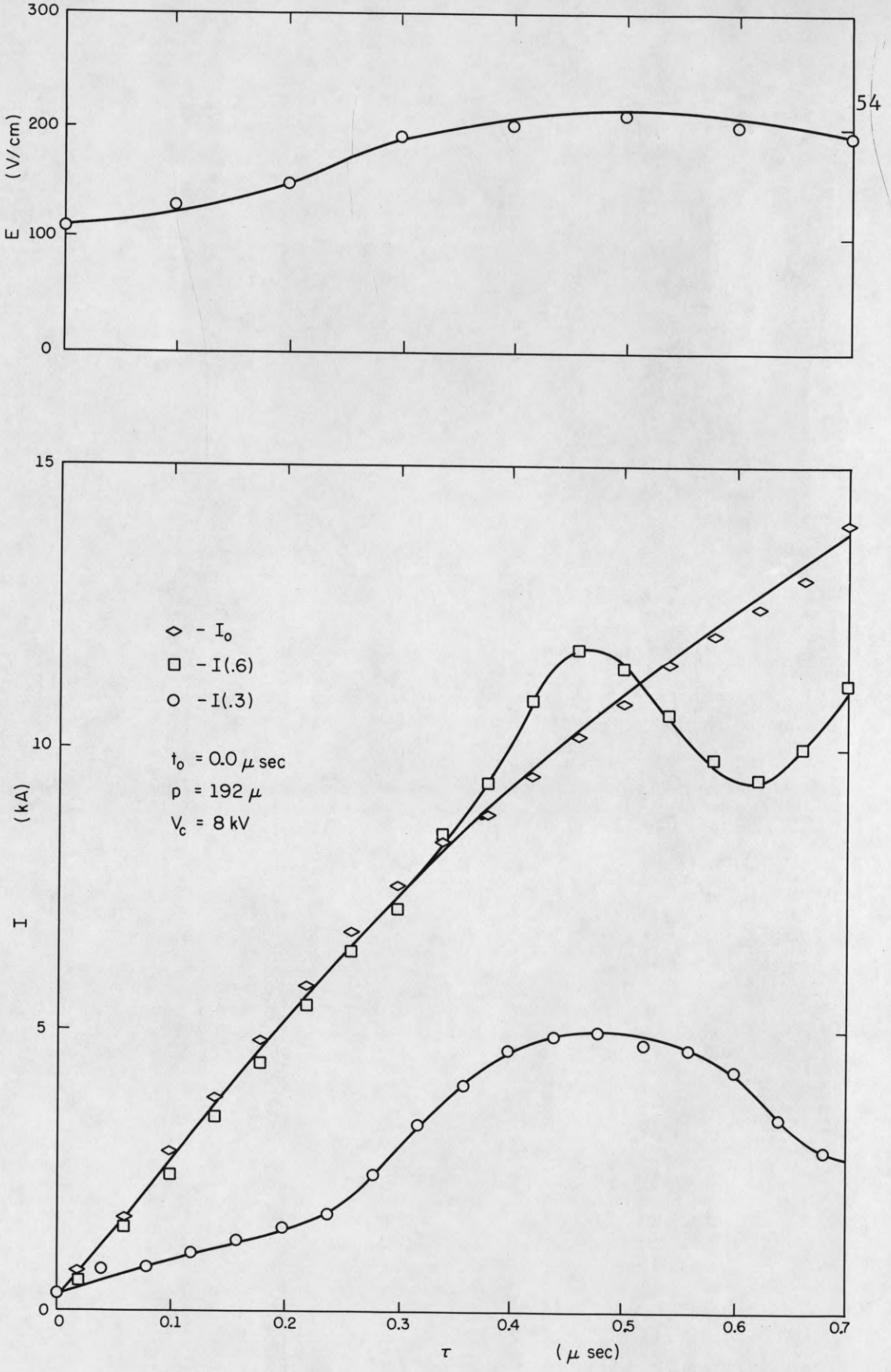

Figure 4.10. Conduction Current and Electric Field at a High Initial Gas Pressure.

At low pressure the ionization is appreciable soon after the conduction current begins to rise. Near the axis of the tube the resistance will be lower since pinching will increase the ratio of n_e to n_o.

The resistivity due to electron-ion collisions is

$$\eta_i = \frac{0.06}{T_e^{3/2}} \simeq 2 \cdot 10^{-5} \ \Omega \text{ cm}$$

for T_e = 200 eV. The resistivity due to electron neutral collisions is

$$\eta_o \simeq \frac{2}{3} \cdot 10^{-3} \frac{n_o}{n_e} \ \Omega \text{ - cm.}$$

Probe measurements to be mentioned later indicate that $n_o/n_e \sim 10^{-1}$ for p = 29 μ. The resistivity of the discharge due to collisions should therefore be of the order of 10^{-4} Ω cm. From the current inside r = 0.3 cm and the electric field shown in Fig. 4.9, the resistivity is about 10^{-2} Ω cm.

Figure 4.11 shows the electric field averaged over $0 \leq \tau \leq \frac{1}{2}$ μs plotted versus pressure for V_c = 8 and 16 kV. The electric field rises for high pressures because ionization is small enough to allow electron-neutral collisions to be important.

In Fig. 4.12 the peak conduction current is plotted versus condensor bank voltage for low pressures. The dotted lines indicate the conduction current obtained from complete ionization and a drift velocity equal to the ion-acoustic velocity for T_e = 200 eV. This seems to give the proper order of magnitude for the current. The gas

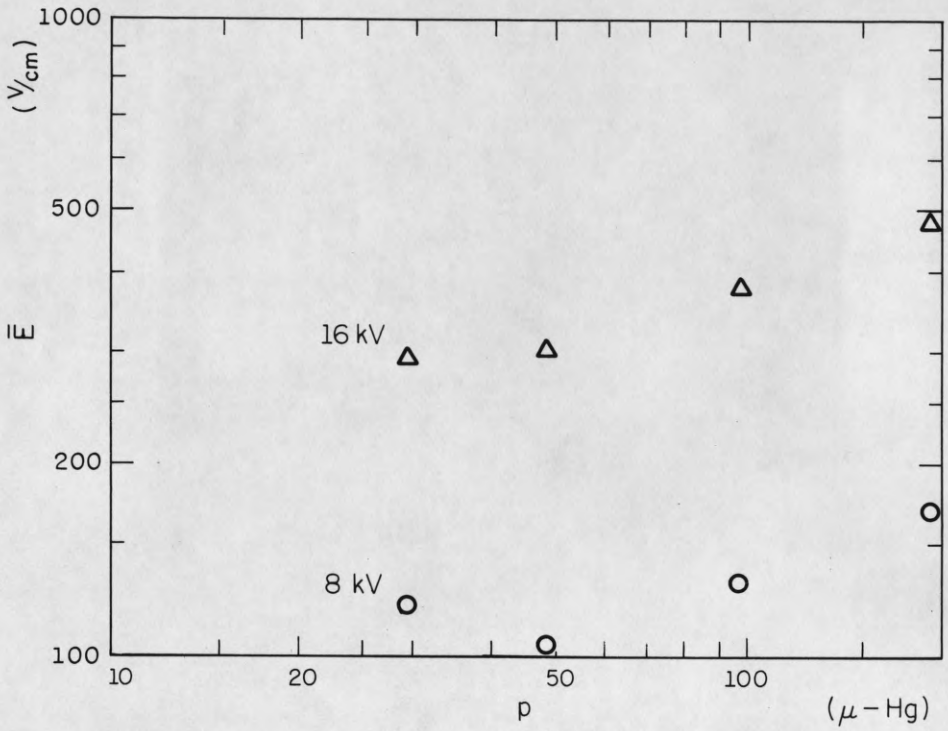

Figure 4.11. Electric Field Averaged Over $0 < \tau < \frac{1}{2}$ μs versus Pressure.

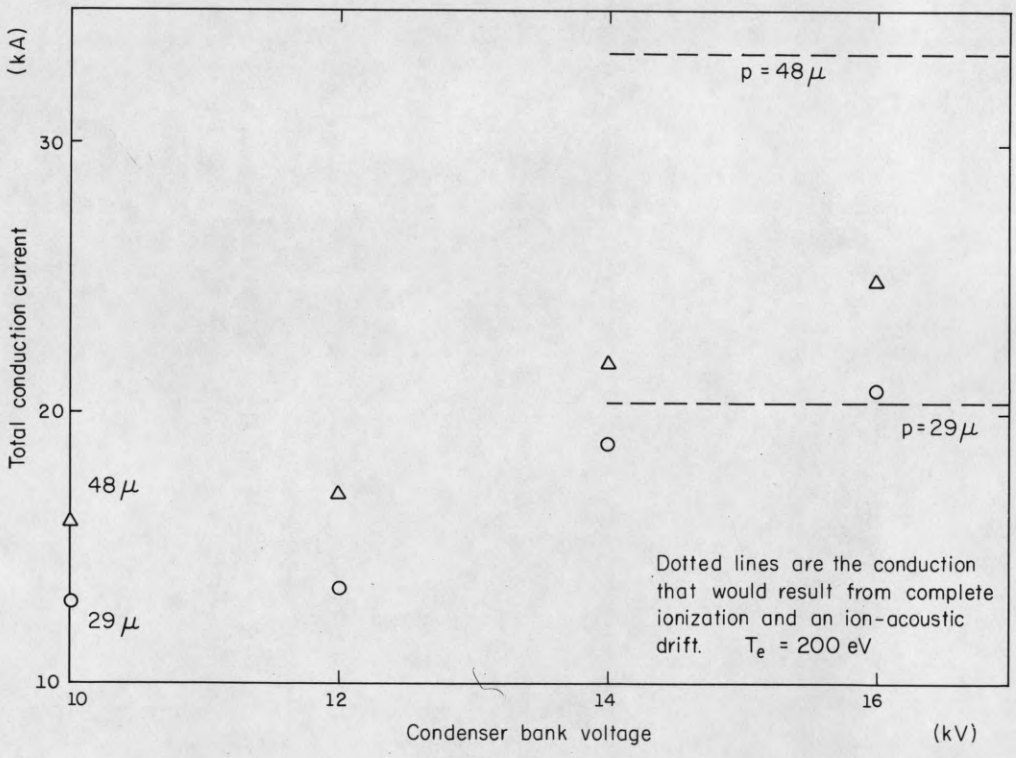

Figure 4.12. Peak Conduction Current Versus Condensor Bank Voltage.

is probably not wholly ionized at low condensor bank voltage or high pressure so the current would be lower. This agreement is only order of magnitude, of course, as the temperature may differ by factors of two from 200 eV as will be seen later.

4.3 Electron Temperature and Density

The measurement of the electron temperature and density was difficult. The density could have been found by the width of hydrogen lines, but unfortunately the lines were too broad for the closest spaced Fabry-Perot etalon available to us, and too narrow for our monochrometer. The densities were too high for microwave measurement. Bremstrahlung was very strong and could have yielded the electron temperature, but unfolding the transmission characteristics of the optical system was prohibitive.

The Langmuir probe (Chen, [13]) was found to give satisfactory results. The probe was placed just inside the tube at the anode end so there would not be large voltage differences to contend with. The probe and associated circuitry are shown in Fig. 4.13.

The probe was made of platinum to lower the likelihood of arcs and large secondary emission currents. A probe of 0.010 inch diameter was tried, but it was destroyed by arcing. The 0.030-inch probe used was pitted from sputtering, but did not change appreciably in size from use. From this, and from the reasonable results we decided that arcing did not take place.

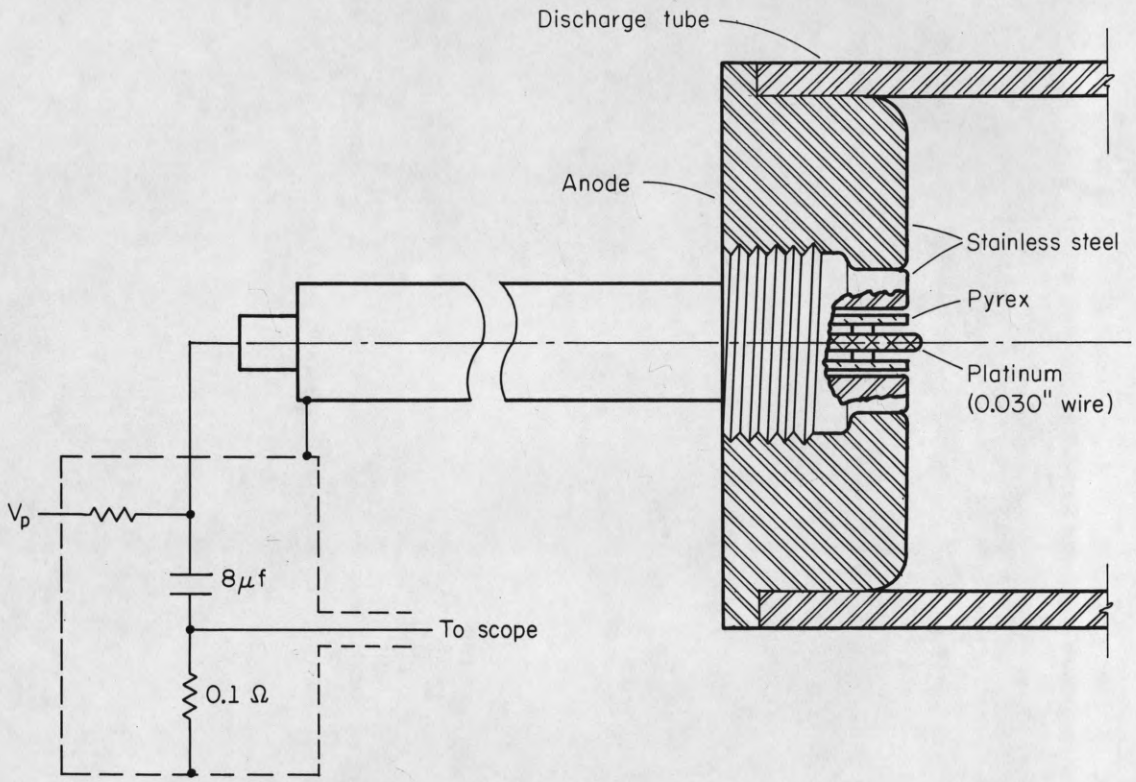

Figure 4.13. Langmuir Probe Experimental Arrangement.

The circuitry for the probe was mounted directly at the end of the system. Stray series resistance was checked and found to be much less than the 0.1 Ω current measuring resistance. In deriving the data the voltage drops across the resistor and condensor were taken into account.

Because of the high densities the ion saturation current was too high to be measurable. For this reason the data had to be taken from a small portion of the probe characteristic. The current to the probe may be written

$$i_p = I_i(e^{V_p/T_e} - 1) \tag{4.3}$$

where V_p is the voltage measured from the floating voltage and I_i is the ion saturation current given by

$$\begin{aligned} I_i &= \frac{1}{2} n_e e A \left(\frac{e T_e}{m_i} \right)^{\frac{1}{2}} \\ &= 0.77 \cdot 10^{-13} A n_e T_e^{\frac{1}{2}} \text{ amps} \end{aligned} \tag{4.4}$$

for the electron density n_e in cm^{-3}, the area of the probe A in cm^2 and the electron temperature T_e in eV. Equation (4.3) is valid as long as i_p is below the electron saturation current, as it is in our case. The magnetic field is not important since the ion gyration radius is large compared to probe. The frequency response of the probe is limited by the ion plasma frequency which is so large (of the order of 1 kMc) in our case as to pose no problem.

For our probe $A = 4 \cdot 10^{-2}$ cm^2. Assuming $n_e \sim 10^{16}$ cm^{-3} and $T_e \sim 10^2$ eV. I_i is on the order of 10^3 amps. This is too high to be easily measured and might destroy the probe. If Eq. (4.3) is approximated by

$$i_p \doteq \frac{I_i}{T_e} V_p + \frac{1}{2} \frac{I_i}{T_e^2} V_p^2, \qquad |V_p| \ll T_e \tag{4.5}$$

both I_i and T_e may be obtained from a small portion of the i_p, V_p characteristic. Equation (4.3) is derived by assuming a Maxwellian electron velocity distribution and an ion current independent of probe voltage. The assumption of constant ion current should be reasonable, but if the plasma is not near complete ionization, the high energy tail of the electron distribution may be effected by ionization. The values n_e and T_e we obtain should be the same as would be obtained by double probe measurements.

Figure 4.14 shows conduction current and probe current traces for three different probe voltages. The voltages shown are not corrected for voltage drops across the resistor and condensor in the probe circuit. The first part of the probe trace is grossly effected by runaway and cannot be used for obtaining n_e and T_e.

Figure 4.15 is an example of the probe characteristic for one set of parameters. Figures 4.16 and 4.17 show the measured electron density and temperature at $t = \frac{1}{2}$ μs versus pressure for V_c = 8 and 10 kV. The temperature is accurate to about 50%. The density is accurate to about 25% relative to other measurements, but only to about 50% absolutely due to uncertainty in the value of the probe area.

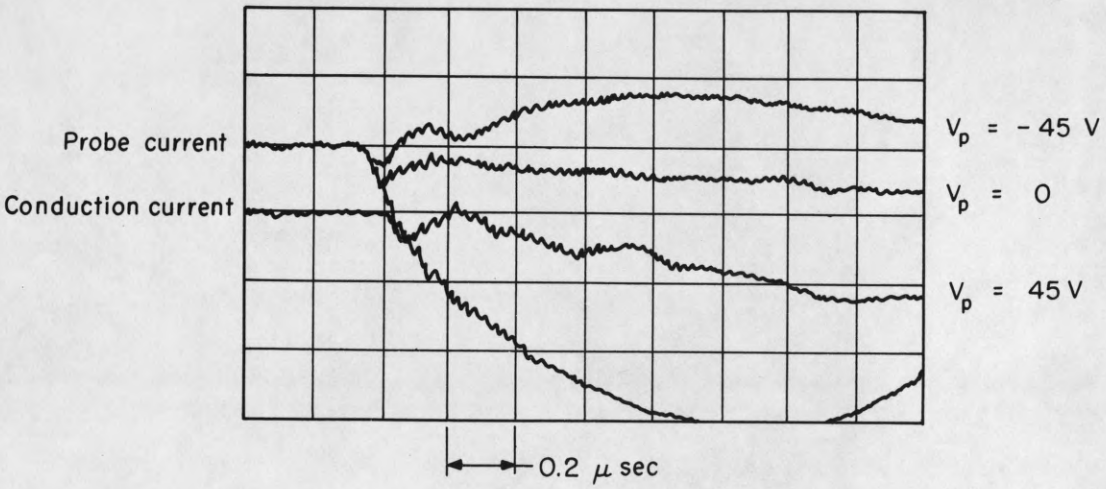

Figure 4.14. Langmuir Probe Current for Several Probe Voltages. Voltages shown are not corrected for circuit impedances.

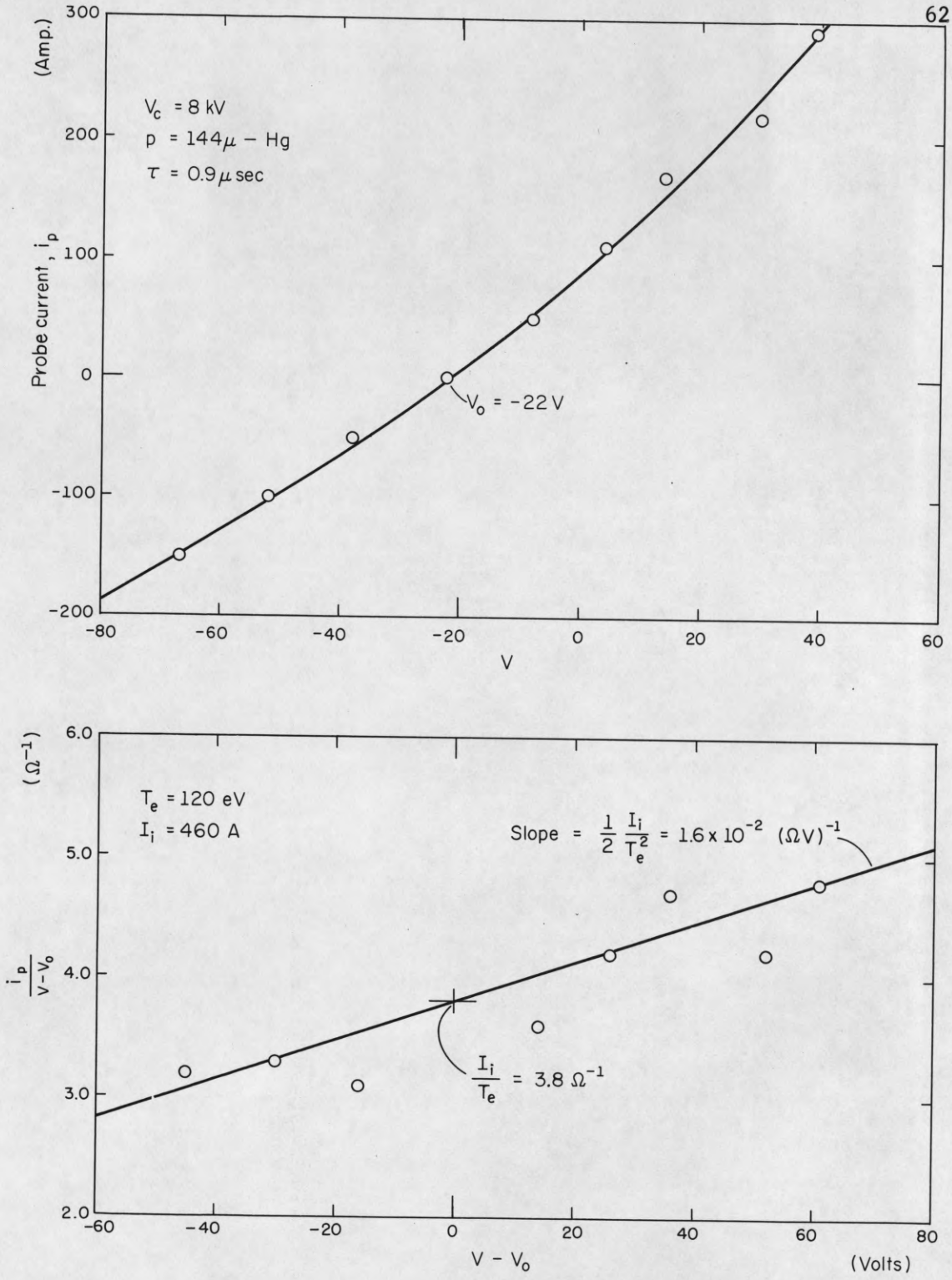

Figure 4.15. Typical Probe Characteristic.

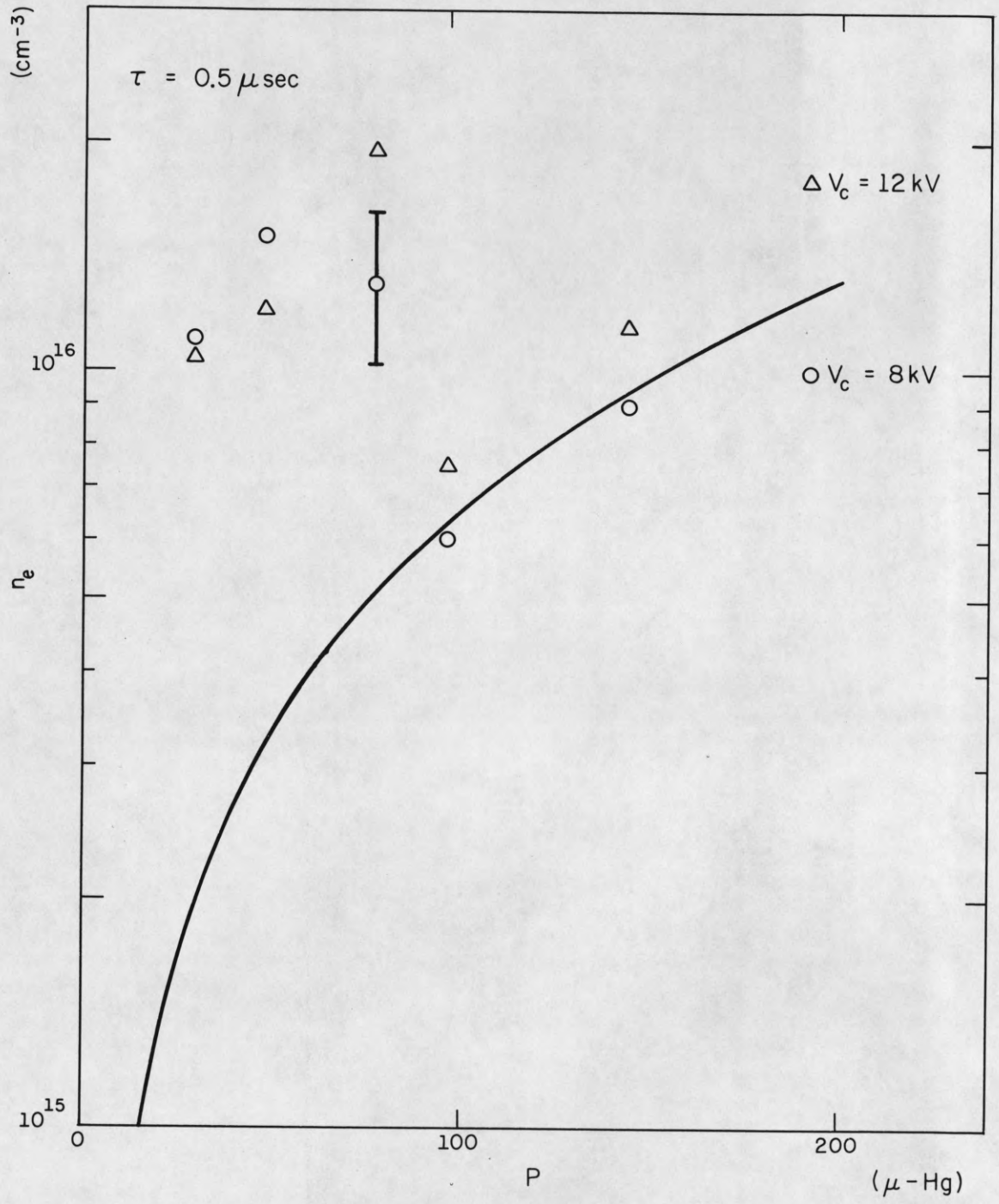

Figure 4.16. Electron Density versus Initial Gas Pressure as Measured by the Langmuir Probe. Solid line represents initial H atom density.

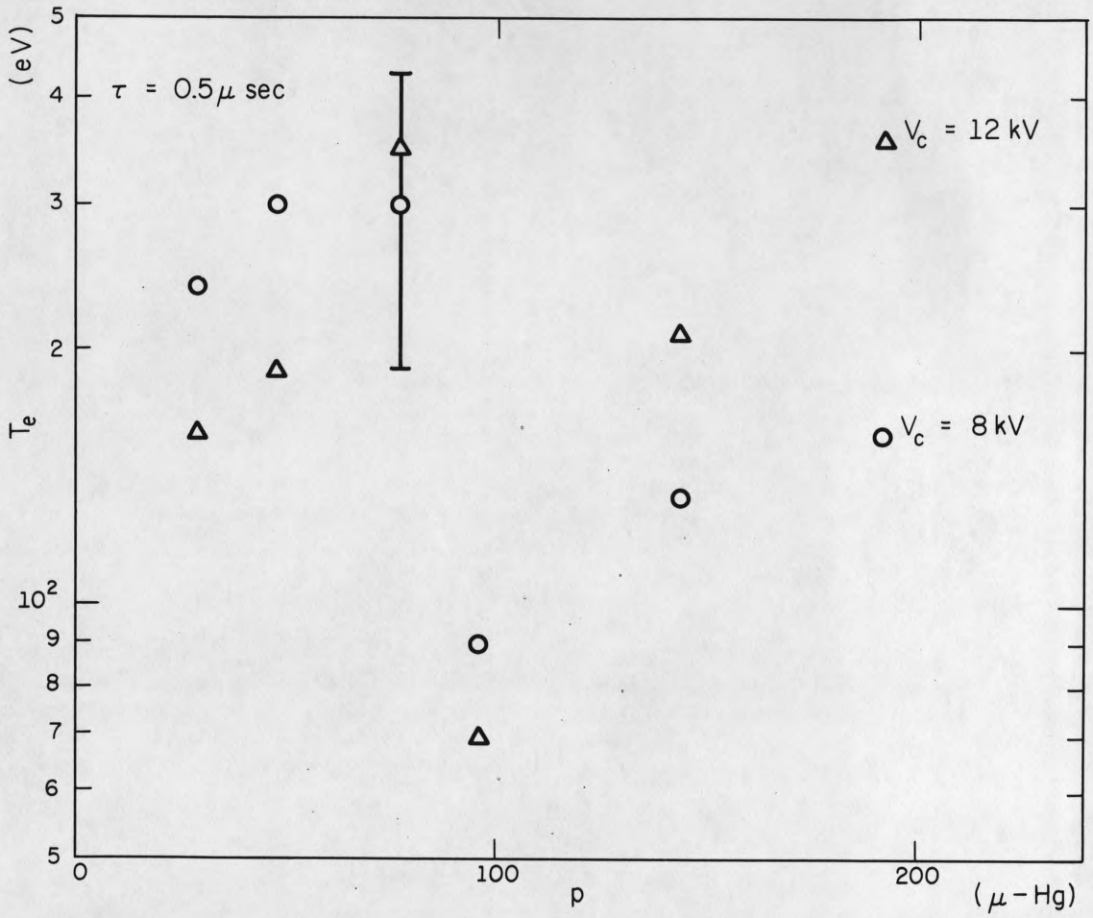

Figure 4.17. Electron Temperature versus Initial Gas Pressure as Measured by the Langmuir Probe.

The solid line represents the initial numbers of H atoms per cm^3, n_o. Since the magnetic probe data indicates a pinched discharge for all cases, the electron density should be a factor of about K^2 above n_o for complete ionization. For pressures below 90 μ-Hg this is seen to be the case (as the magnetic probe indicates $K \sim 3$) but at higher pressures it is not. The magnetic probe data also indicated different behavior at low and high pressure, as can be seen by comparing Figs. 3.9 and 4.10. The current near the axis, I(0.3), always leveled off to a constant value soon after $\tau = o$ for low pressure.

We believe that the discharge is nearly completely ionized below $p = 90\ \mu \sim$ Hg, but not above. The lack of complete ionization may have disturbed the electron distribution enough that the probe measurements are inaccurate at the higher pressures.

Probe measurements were not made at higher condensor bank voltages for technical reasons.

4.4 Plasma Oscillations

We made a considerable effort to obtain the spectrum of the plasma oscillation, but failed to get quantitative results for various technical reasons. We did, however, find that strong low frequency oscillations ($\sim$ 50 Mc) did arise shortly after conduction became large, and continued to be present throughout times of interest. Figure 4.18 shows the 30 Mc oscillation amplitude taken from the Langmuir probe. By putting an X-band cavity directly at the Langmuir probe output, it was found that high frequency oscillations ($\sim 10^4$ Mc) occured just as

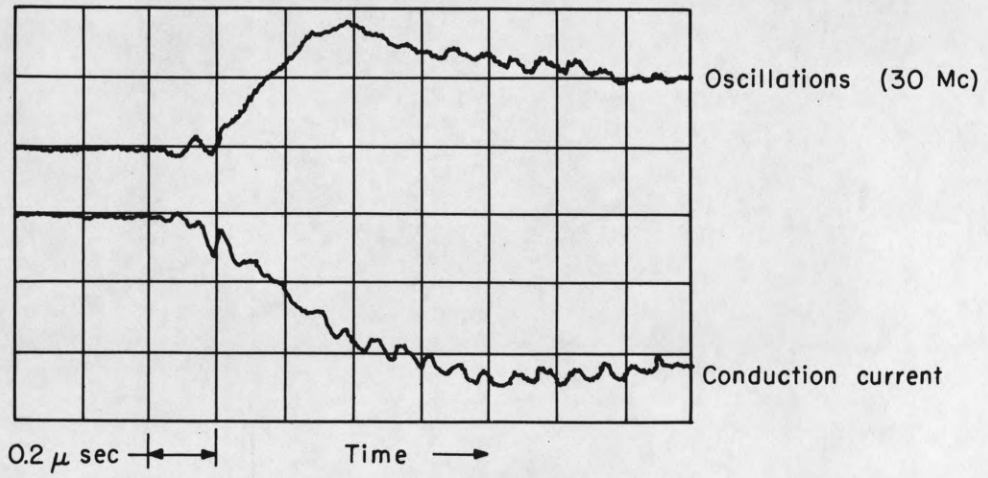

Figure 4.18. 30 Mc Oscillation Amplitude versus Time for V_c = 10 kV, p = 48 μ-Hg.

the runaway began to disappear, and then decayed away as the runaway did. This decay was much longer than the Q of the cavity would have given.

5. Conclusion

A dense, hot plasma was generated, and was quite reproducible considering the very fast time scale on which the experiment was performed. The magnetic probe measurements indicated that a constricted discharge of about 1/3 of the tube radius built up and was reasonably stable for times of interest. Current densities were very high ($\sim$ 40 kA/cm^2) and at low pressures agreed in order of magnitude with the ion-acoustic drift found in the simple moment theory calculations of Field and Fried.[11] It should be pointed out, however, that at lower pressures than we used, Suprunenko et al [6] found much higher current densities than ion-acoustic drift would indicate. We still believe that ion-acoustic oscillations limit our current, since strong low frequency oscillations are found, and since the measured resistivities are 3 orders of magnitude above the collisional values.

The electron densities measured were quite reasonable, and while the temperatures were several times those found in other experiments of this sort, this could be explained by the much higher current densities ($\sim$ 40 kA/cm^2 compared to $\sim$ 5 kA/cm^2 in the case of Suprunenko et al, for instance). We believe these temperatures must be approximately correct. Recent turbulent heating experiments* have yielded similarly high resistivities and electron temperatures. Our measurements indicate critical electric fields of about 100 V/cm.

---

*Fanchenko et al,[14] Demidov et al.[15]

Fairly strong electron runaway was found for a very short time. The Faraday runaway pickup indicated a total runaway of the order of 1 amp for velocities within two degrees of the machine axis. Appreciable currents were found at larger angle. While the runaway disappears as the density builds up, the electric field remains greater than the critical electric field so we do not believe the high density causes the cessation of runaway. High frequency oscillations ($\sim 10^{10}$ Hz) disappear as the runaway disappears, whereas low frequency oscillations ($\sim 10^{7}$ - 10^{8} Hz) continue through times of interest. The electron plasma frequency ($\sim 10^{12}$ Hz) was too high to examine. We do not know therefore, whether electron plasma oscillations are involved in the continued stoppage of runaway electrons. To the best of our knowledge, it has not been shown theoretically whether the electron distribution divides into two streams, or whether it merely spreads out greatly in the direction of the electric field under the influence of an electric field and collisions, but no spacial inhomogeneity. If ion-acoustic waves alone prevent additional runaway, the fast electrons would have to interact with the slow ion-acoustic waves moving at almost 90^{o} to their path.* This would mean a large deflection rather than a large deceleration. Large effects due to k vectors at large angles to the electric field were predicted by Field and Fried.

---

*The electron velocity component along the waves k vector must equal the phase velocity for strong interaction.

Bibliography

[1] Budker, G. J., "Relativistic Stabilized Electron Beam I," Cern Symposium 1, G8 (1956).

Budker, G. J., and A. A. Naumov, "Relativistic Stabilized Electron Beam II," Cern Symposium 1, 76 (1956).

[2] Skarsgard, H. M., A. R. Strilchuk, and W. W. Zuzak, "Wave Plasma Interactions Involving Intense Runaway Electron Streams," Proceedings of the Seventh International Conference on Phenomena in Ionized Gases, Belgrade, 1965.

[3] Rogers, K. C., S. J. Lukasik, and L. Ferrari, "Megatron Final Report," Stevens Institute of Technology, p. 147 (5/65).

[4] Grossmann-Doerth, U. and J. Junker, "Runaway Electrons in a Toroidal Z-Pinch Discharge in Hydrogen," Neuclear Fusion: 1962 Supplement, Part 3, p. 1007.

[5] Drees, J. and W. Paul, "Beschleunigung von Elektronen in einem Plasmabetatron," Zeitschrift fur Physik 180, 340 (1964).

[6] Suprunenko, V. A., E. A. Sukhomlin, and N. I. Reva, "Ohmic Heating and the Electrical Conductivity of a Plasma in Strong Electric Fields," Plasma Physics (Journal of Nuclear Energy, Part C) 7, 297 (1965).

[7] Dreicer, H., "Electron and Ion Runaway in a Fully Ionized Gas, I," Physical Review 115, 238 (1959).

[8] Dreicer, H., "Electron and Ion Runaway in a Fully Ionized Gas, II," Physical Review 117, 329 (1960).

[9] Kruskal, M. D. and I. B. Bernstein, "Runaway Electrons in an Ideal Lorentz Plasma," Physics of Fluids 7, 407 (1964).

[10] Drummond, W. E. and D. Pines, "Nonlinear Stability of Plasma Oscillations," Nuclear Fusion: 1962 Supplement, Part 3, p. 1049.

[11] Field, E. C. and B. D. Fried, "Solution of the Kinetic Equation for an Unstable Plasma in an Electric Field," Physics of Fluids 7, 1937 (1964).

[12] Kerst, P. W., "A High Current Linear Accelerator Experiment," General Atomic Report GAMD-1349.

Brower, D. F. and D. W. Kerst, "A Method of Coupling Voltage Sources to Gaseous Discharge Tubes With Other Applications Accelerators," General Atomic Report GAMD-315.

[13] Chen, F. F., "Plasma Diagnostic Techniques," Chapter 4, Edited by R. H. Huddlestone and S. L. Leonard, Academic Press, 1965.

[14] Franchenko, S. D., B. A. Demidov, N. I. Elagin, and D. D. Ryutov, "Absorption of Energy Produced by the Two-Stream Instability in a Toroidal Plasma," Soviet Physics JETP 19, 337 (1964).

[15] Demidov, B. A., N. I. Elagin, D. D. Ryutov, and S. D. Franchenko, "Anomolous Resistance and Microwave Radiation from a Plasma in a Strong Electric Field," Soviet Physics, JETP 21, 302 (1965).

Vita

I, Clifford William Mendel, Jr., was born on August 27, 1936 of Professor of Mathematics Clifford William Mendel, Sr. and Elisabeth Evans Mendel in Cincinnati, Ohio. My elementary education was received in the public school system at Urbana, Illinois. I graduated from Urbana High School in June of 1954. In the Fall of 1954 I began studies in Engineering Physics at the University of Illinois, and received my B.S. degree there in February, 1959. During the time I spent in high school and as an undergraduate in college, I had several jobs dealing mostly with electronics. I continued on at the University of Illinois in graduate school, obtaining my M.S. in Physics in August of 1959. In the Summer of 1959 I began working at the Coordinated Science Laboratory doing computer research on the spectrum of water waves with Professor Bruce Hicks. In 1960 I began Plasma Physics research with Professor Manfred Raether. The Summer of 1962 was spent at the Summer Institute on Plasma Physics at Princeton University.

Distribution list as of May 1, 1966

1 Dr. Edward M. Reilley
Asst. Director (Research)
Ofc. of Defense Res. & Engrg.
Department of Defense
Washington, D. C. 20301

1 Office of Deputy Director
(Research and Information Rm 3D1037)
Department of Defense
The Pentagon
Washington, D. C. 20301

1 Director
Advanced Research Projects Agency
Department of Defense
Washington, D. C. 20301

1 Director for Materials Sciences
Advanced Research Projects Agency
Department of Defense
Washington, D. C. 20301

1 Headquarters
Defense Communications Agency (333)
The Pentagon
Washington, D. C. 20305

20 Defense Documentation Center
Attn: TISIA
Cameron Station, Building 5
Alexandria, Virginia 22314

1 Director
National Security Agency
Attn: Librarian C-332
Fort George G. Meade, Maryland 20755

1 Weapons Systems Evaluation Group
Attn: Col. Finis G. Johnson
Department of Defense
Washington, D. C. 20305

1 National Security Agency
Attn: R4-James Tippet
Office of Research
Fort George G. Meade, Maryland 20755

1 Central Intelligence Agency
Attn: OCR/DD Publications
Washington, D. C. 20505

1 AFRSTE
Hqs. USAF
Room 1D-429, The Pentagon
Washington, D. C. 20330

1 AUL3T-9663
Maxwell Air Force Base, Alabama 36112

1 AFFTC (FTBPP-2)
Technical Library
Edwards AFB, California 93523

1 Space Systems Division
Air Force Systems Command
Los Angeles Air Force Station
Los Angeles, California 90045
Attn: SSSD

1 SSD(SSTRT/Lt. Starbuck)
AFUPO
Los Angeles, California 90045

1 Det. #6, OAR (LOOAR)
Air Force Unit Post Office
Los Angeles, California 90045

1 Systems Engineering Group (RTD)
Technical Information Reference Branch
Attn. SEPIR
Directorate of Engineering Standards
& Technical Information
Wright-Patterson AFB, Ohio 45433

1 ARL (ARIY)
Wright-Patterson AFB, Ohio 45433

1 AFAL (AVT)
Wright-Patterson AFB, Ohio 45433

1 AFAL (AVTE/R. D. Larson)
Wright-Patterson AFB, Ohio 45433

1 Office of Research Analyses
Attn: Technical Library Branch
Holloman AFB, New Mexico 88330

2 Commanding General
Attn: STEWS-WS-VT
White Sands Missile Range
New Mexico 88002

1 RADC (EMLAL-I)
Griffiss AFB, New York 13442
Attn: Documents Library

1 Academy Library (DFSLB)
U. S. Air Force Academy
Colorado 80840

1 FJSRL
USAF Academy, Colorado 80840

1 APGC (PGBPS-12)
Eglin AFB, Florida 32542

1 AFETR Technical Library
(ETV, MU-135)
Patrick AFB, Florida 32925

1 AFETR (ETLLG-I)
STINFO Officer (for Library)
Patrick AFB, Florida 32925

1 AFCRL (CRMXLR)
AFCRL Research Library, Stop 29
L. G. Hanscom Field
Bedford, Massachusetts 01731

2 ESD (ESTI)
L. G. Hanscom Field
Bedford, Massachusetts 01731

1 AEDC (ARO, INC)
Attn: Library/Documents
Arnold AFS, Tennessee 37389

2 European Office of Aerospace Research
Shell Building
47 Rue Cantersteen
Brussels, Belgium

5 Lt. Col. E. P. Gaines, Jr.
Chief, Electronics Division
Directorate of Engineering Sciences
Air Force Office of Scientific Research
Washington, D. C. 20333

1 U. S. Army Research Office
Attn. Physical Sciences Division
3045 Columbia Pike
Arlington, Virginia 22204

1 Research Plans Office
U. S. Army Research Office
3045 Columbia Pike
Arlington, Virginia 22204

1 Commanding General
U. S. Army Materiel Command
Attn: AMCRD-RS-PE-E
Washington, D. C. 20315

1 Commanding General
U. S. Army Strategic Communications Command
Washington, D. C. 20315

1 Commanding Officer
U. S. Army Materials Research Agency
Watertown Arsenal
Watertown, Massachusetts 02172

1 Commanding Officer
U. S. Army Ballistics Research Laboratory
Attn: V. W. Richards
Aberdeen Proving Ground
Aberdeen, Maryland 21005

1 Commandant
U. S. Army Air Defense School
Attn: Missile Sciences Division C&S Dept.
P. O. Box 9390
Fort Bliss, Texas 79916

1 Commanding General
U. S. Army Missile Command
Attn: Technical Library
Redstone Arsenal, Alabama 35809

1 Commanding General
Frankford Arsenal
Attn: SMUFA-L6000 (Dr. Sidney Ross)
Philadelphia, Pennsylvania 19137

1 U. S. Army Munitions Command
Attn: Technical Information Branch
Picatinney Arsenal
Dover, New Jersey 07801

1 Commanding Officer
Harry Diamond Laboratories
Attn: Mr. Berthold Altman
Connecticut Avenue & Van Ness Street N. W.
Washington, D. C. 20438

1 Commanding Officer
U. S. Army Security Agency
Arlington Hall
Arlington, Virginia 22212

1 Commanding Officer
U. S. Army Limited War Laboratory
Attn: Technical Director
Aberdeen Proving Ground
Aberdeen, Maryland 21005

1 Commanding Officer
Human Engineering Laboratories
Aberdeen Proving Ground, Maryland 21005

1 Director
U. S. Army Engineer Geodesy, Intelligence
and Mapping
Research and Development Agency
Fort Belvoir, Virginia 22060

1 Commandant
U. S. Army Command and General Staff College
Attn: Secretary
Fort Leavenworth, Kansas 66270

1 Dr. H. Robl, Deputy Chief Scientist
U. S. Army Research Office (Durham)
Box CM, Duke Station
Durham, North Carolina 27706

1 Commanding Officer
U. S. Army Research Office (Durham)
Attn: CRD-AA-IP (Richard O. Ulsh)
Box CM, Duke Station
Durham, North Carolina 27706

1 Superintendent
U. S. Army Military Academy
West Point, New York 10996

1 The Walter Reed Institute of Research
Walter Reed Medical Center
Washington, D. C. 20012

1 Commanding Officer
U. S. Army Electronics R&D Activity
Fort Huachuca, Arizona 85163

1 Commanding Officer
U. S. Army Engineer R&D Laboratory
Attn: STINFO Branch
Fort Belvoir, Virginia 22060

1 Commanding Officer
U. S. Army Electronics R&D Activity
White Sands Missile Range, New Mexico 88002

1 Dr. S. Benedict Levin, Director
Institute for Exploratory Research
U. S. Army Electronics Command
Fort Monmouth, New Jersey 07703

1 Director
Institute for Exploratory Research
U. S. Army Electronics Command
Attn: Mr. Robert O. Parker, Executive
Secretary, JSTAC (AMSEL-XL-D)
Fort Monmouth, New Jersey 07703

1 Commanding General
U. S. Army Electronics Command
Fort Monmouth, New Jersey 07703

Attn: AMSEL-SC
RD-D
RD-G
RD-GF
RD-MAF-I
RD-MAT
XL-D
XL-E
XL-C
XL-S
HL-D
HL-L
HL-J
HL-P
HL-O
HL-R
NL-D
NL-A
NL-P
NL-R
NL-S
KL-D
KL-E
KL-S
KL-T
VL-D
WL-D

3 Chief of Naval Research
Department of the Navy
Washington, D. C. 20360
Attn: Code 427

4 Chief, Bureau of Ships
Department of the Navy
Washington, D. C. 20360

3 Chief, Bureau of Weapons
Department of the Navy
Washington, D. C. 20360

2 Commanding Officer
Office of Naval Research Branch Office
Box 39, Navy No. 100 F.P.O.
New York, New York 09510

3 Commanding Officer
Office of Naval Research Branch Office
219 South Dearborn Street
Chicago, Illinois 60604

1 Commanding Officer
Office of Naval Research Branch Office
1030 East Green Street
Pasadena, California

1 Commanding Officer
Office of Naval Research Branch Office
207 West 24th Street
New York, New York 10011

Distribution list as of May 1, 1966 (cont'd.)

1 Commanding Officer
Office of Naval Research Branch Office
495 Summer Street
Boston, Massachusetts 02210

8 Director, Naval Research Laboratory
Technical Information Officer
Washington, D. C.
Attn: Code 2000

1 Commander
Naval Air Development and Material Center
Johnsville, Pennsylvania 18974

2 Librarian
U. S. Naval Electronics Laboratory
San Diego, California 95152

1 Commanding Officer and Director
U. S. Naval Underwater Sound Laboratory
Fort Trumbull
New London, Connecticut 06840

1 Librarian
U. S. Navy Post Graduate School
Monterey, California

1 Commander
U. S. Naval Air Missile Test Center
Point Magu, California

1 Director
U. S. Naval Observatory
Washington, D. C.

2 Chief of Naval Operations
OP-07
Washington, D. C.

1 Director, U. S. Naval Security Group
Attn: G43
3801 Nebraska Avenue
Washington, D. C.

2 Commanding Officer
Naval Ordnance Laboratory
White Oak, Maryland

1 Commanding Officer
Naval Ordnance Laboratory
Corona, California

1 Commanding Officer
Naval Ordnance Test Station
China Lake, California

1 Commanding Officer
Naval Avionics Facility
Indianapolis, Indiana

1 Commanding Officer
Naval Training Device Center
Orlando, Florida

1 U. S. Naval Weapons Laboratory
Dahlgren, Virginia

1 Weapons Systems Test Division
Naval Air Test Center
Patuxtent River, Maryland
Attn: Library

1 Mr. Charles F. Yost
Special Assistant to the Director of Research
National Aeronautics and Space Administration
Washington, D. C. 20546

1 Dr. H. Harrison, Code RRE
Chief, Electrophysics Branch
National Aeronautics and Space Administration
Washington, D. C. 20546

1 Goddard Space Flight Center
National Aeronautics and Space Administration
Attn: Library, Documents Section Code 252
Greenbelt, Maryland 20771

1 NASA Lewis Research Center
Attn: Library
21000 Brookpark Road
Cleveland, Ohio 44135

1 National Science Foundation
Attn: Dr. John R. Lehmann
Division of Engineering
1800 G Street, N. W.
Washington, D. C. 20550

1 U. S. Atomic Energy Commission
Division of Technical Information Extension
P. O. Box 62
Oak Ridge, Tennessee 37831

1 Los Alamos Scientific Laboratory
Attn: Reports Library
P. O. Box 1663
Los Alamos, New Mexico 87544

2 NASA Scientific & Technical Information Facility
Attn: Acquisitions Branch (S/AK/DL)
P. O. Box 33
College Park, Maryland 20740

1 Director
Research Laboratory of Electronics
Massachusetts Institute of Technology
Cambridge, Massachusetts 02139

1 Polytechnic Institute of Brooklyn
55 Johnson Street
Brooklyn, New York 11201
Attn: Mr. Jerome Fox
Research Coordinator

1 Director
Columbia Radiation Laboratory
Columbia University
538 West 120th Street
New York, New York 10027

1 Director
Coordinated Science Laboratory
University of Illinois
Urbana, Illinois 61801

1 Director
Stanford Electronics Laboratories
Stanford University
Stanford, California

1 Director
Electronics Research Laboratory
University of California
Berkeley 4, California

1 Director
Electronic Sciences Laboratory
University of Southern California
Los Angeles, California 90007

1 Professor A. A. Dougal, Director
Laboratories for Electronics and
Related Sciences Research
University of Texas
Austin, Texas 78712

1 Division of Engineering and Applied Physics
210 Pierce Hall
Harvard University
Cambridge, Massachusetts 02138

1 Aerospace Corporation
P. O. Box 95085
Los Angeles, California 90045
Attn: Library Acquisitions Group

1 Professor Nicholas George
California Institute of Technology
Pasadena, California

1 Aeronautics Library
Graduate Aeronautical Laboratories
California Institute of Technology
1201 E. California Boulevard
Pasadena, California 91109

1 Director, USAF Project RAND
Via: Air Force Liaison Office
The RAND Corporation
1700 Main Street
Santa Monica, California 90406
Attn: Library

1 The Johns Hopkins University
Applied Physics Laboratory
8621 Georgia Avenue
Silver Spring, Maryland
Attn: Boris W. Kuvshinoff
Document Librarian

1 Hunt Library
Carnegie Institute of Technology
Schenley Park
Pittsburgh, Pennsylvania 15213

1 Dr. Leo Young
Stanford Research Institute
Menlo Park, California

1 Mr. Henry L. Bachmann
Assistant Chief Engineer
Wheeler Laboratories
122 Cuttermill Road
Great Neck, New York

1 University of Liege
Electronic Department
Mathmatics Institute
15, Avenue Des Tilleuls
Val-Benoit, Liege
Belgium

1 School of Engineering Sciences
Arizona State University
Tempe, Arizona

1 University of California at Los Angeles
Department of Engineering
Los Angeles, California

1 California Institute of Technology
Pasadena, California
Attn: Documents Library

1 University of California
Santa Barbara, California
Attn: Library

1 Carnegie Institute of Technology
Electrical Engineering Department
Pittsburgh, Pennsylvania

1 University of Michigan
Electrical Engineering Department
Ann Arbor, Michigan

1 New York University
College of Engineering
New York, New York

1 Syracuse University
Department of Electrical Engineering
Syracuse, New York

1 Yale University
Engineering Department
New Haven, Connecticut

1 Airborne Instruments Laboratory
Deerpark, New York

1 Bendix Pacific Division
11600 Sherman Way
North Hollywood, California

1 General Electric Company
Research Laboratories
Schenectady, New York

1 Lockheed Aircraft Corporation
P. O. Box 504
Sunnyvale, California

1 Raytheon Company
Bedford, Massachusetts
Attn: Librarian

Security Classification

DOCUMENT CONTROL DATA R&D

(Security classification of title, body of abstract and indexing annotation must be entered when the overall report is classified)

1. ORIGINATING ACTIVITY (Corporate author)

University of Illinois
Coordinated Science Laboratory
Urbana, Illinois 61801

2a. REPORT SECURITY CLASSIFICATION

Unclassified

2b. GROUP

3. REPORT TITLE

INVESTIGATION OF DENSE PLASMA UNDER A STRONG ELECTRIC FIELD

4. DESCRIPTIVE NOTES (Type of report and inclusive dates)

5. AUTHOR(S) (Last name, first name, initial)

Mendel, Clifford W., Jr.

6. REPORT DATE

May, 1966

7a TOTAL NO. OF PAGES

72

7b. NO. OF REFS.

15

8a. CONTRACT OR GRANT NO.

DA 28 043 AMC 00073(E)

b. PROJECT NO.

20014501B31F

c.

d.

9a. ORIGINATOR'S REPORT NUMBER(S)

R-289

9b. OTHER REPORT NO(S) (Any other numbers that may be assigned this report)

10. AVAILABILITY/LIMITATION NOTICES

Distribution of this report is unlimited.

11. SUPPLEMENTARY NOTES

Ph.D. Thesis, Department of Physics, Univ. of Illinois

12. SPONSORING MILITARY ACTIVITY

Joint Services Electronics Program thru U. S. Army Electronics Command Fort Monmouth, New Jersey 07703

13. ABSTRACT

A hydrogen plasma of density $\sim 10^{16}$ cm^{-3} and electron temperature $\sim$ 200 eV has been investigated under electric fields of 100 to 500 V/cm. A pinch of pinch ratio $\sim$ 3 was found to be hydrodynamically stable for $\sim 2\mu$s during which the experiment was performed. A sharp burst of runaway electrons of total current of the order of amperes occurred and disappeared shortly after conduction began. Large low frequency oscillations believed to be ion-acoustic oscillations appear and give rise to very high resistivities in qualitative agreement with recent theories on plasma conductivity. (Author)

DD FORM 1 JAN 64 1473

Security Classification

Security Classification

KEY WORDS	LINK A		LINK B		LINK C	
	ROLE	WT	ROLE	WT	ROLE	WT
plasma physics dense plasma electron runaway turbulent resistance						

INSTRUCTIONS

1. ORIGINATING ACTIVITY: Enter the name and address of the contractor, subcontractor, grantee, Department of Defense activity or other organization (corporate author) issuing the report.

2a. REPORT SECURITY CLASSIFICATION: Enter the overall security classification of the report. Indicate whether "Restricted Data" is included. Marking is to be in accordance with appropriate security regulations.

2b. GROUP: Automatic downgrading is specified in DoD Directive 5200.10 and Armed Forces Industrial Manual. Enter the group number. Also, when applicable, show that optional markings have been used for Group 3 and Group 4 as authorized.

3. REPORT TITLE: Enter the complete report title in all capital letters. Titles in all cases should be unclassified. If a meaningful title cannot be selected without classification, show title classification in all capitals in parenthesis immediately following the title.

4. DESCRIPTIVE NOTES: If appropriate, enter the type of report, e.g., interim, progress, summary, annual, or final. Give the inclusive dates when a specific reporting period is covered.

5. AUTHOR(S): Enter the name(s) of author(s) as shown on or in the report. Enter last name, first name, middle initial. If military, show rank and branch of service. The name of the principal author is an absolute minimum requirement.

6. REPORT DATE: Enter the date of the report as day, month, year; or month, year. If more than one date appears on the report, use date of publication.

7a. TOTAL NUMBER OF PAGES: The total page count should follow normal pagination procedures, i.e., enter the number of pages containing information.

7b. NUMBER OF REFERENCES: Enter the total number of references cited in the report.

8a. CONTRACT OR GRANT NUMBER: If appropriate, enter the applicable number of the contract or grant under which the report was written.

8b, 8c, & 8d. PROJECT NUMBER: Enter the appropriate military department identification, such as project number, subproject number, system numbers, task number, etc.

9a. ORIGINATOR'S REPORT NUMBER(S): Enter the official report number by which the document will be identified and controlled by the originating activity. This number must be unique to this report.

9b. OTHER REPORT NUMBER(S): If the report has been assigned any other report numbers (either by the originator or by the sponsor), also enter this number(s).

10. AVAILABILITY/LIMITATION NOTICES: Enter any limitations on further dissemination of the report, other than those imposed by security classification, using standard statements such as:

(1) "Qualified requesters may obtain copies of this report from DDC."

(2) "Foreign announcement and dissemination of this report by DDC is not authorized."

(3) "U. S. Government agencies may obtain copies of this report directly from DDC. Other qualified DDC users shall request through

_____."

(4) "U. S. military agencies may obtain copies of this report directly from DDC. Other qualified users shall request through

_____."

(5) "All distribution of this report is controlled. Qualified DDC users shall request through

_____."

If the report has been furnished to the Office of Technical Services, Department of Commerce, for sale to the public, indicate this fact and enter the price, if known.

11. SUPPLEMENTARY NOTES: Use for additional explanatory notes.

12. SPONSORING MILITARY ACTIVITY: Enter the name of the departmental project office or laboratory sponsoring (paying for) the research and development. Include address.

13. ABSTRACT: Enter an abstract giving a brief and factual summary of the document indicative of the report, even though it may also appear elsewhere in the body of the technical report. If additional space is required, a continuation sheet shall be attached.

It is highly desirable that the abstract of classified reports be unclassified. Each paragraph of the abstract shall end with an indication of the military security classification of the information in the paragraph, represented as (TS), (S), (C), or (U).

There is no limitation on the length of the abstract. However, the suggested length is from 150 to 225 words.

14. KEY WORDS: Key words are technically meaningful terms or short phrases that characterize a report and may be used as index entries for cataloging the report. Key words must be selected so that no security classification is required. Identifiers, such as equipment model designation, trade name, military project code name, geographic location, may be used as key words but will be followed by an indication of technical context. The assignment of links, roles, and weights is optional.

DD FORM 1 JAN 64 1473

Security Classification